Formation of highly oxygenated organic molecules from aromatic compounds.

Ugo Molteni[1], Federico Bianchi[2], Felix Klein[1], Imad El Haddad[1], Carla Frege[1], Michel J. Rossi[1], Josef Dommen[1], Urs Baltensperger[1,*]

[1]Laboratory of Atmospheric Chemistry, Paul Scherrer Institute, CH-5232 Villigen, Switzerland
[2]Department of Physics, University of Helsinki, 00014 Helsinki, Finland

Correspondence to: Urs Baltensperger (urs.baltensperger@psi.ch)

Abstract

Anthropogenic volatile organic compounds (AVOC) often dominate the urban atmosphere and consist to a large degree of aromatic hydrocarbons (ArHC), such as benzene, toluene, xylenes, and trimethylbenzenes, e.g. from handling and combustion of fuels. These compounds are important precursors for the formation of secondary organic aerosol. Here we show that oxidation of aromatics with OH leads to a subsequent autoxidation chain reaction forming highly oxygenated molecules (HOMs) with an O:C ratio of up to 1.09. This is exemplified for five single-ring ArHC (benzene, toluene, o-/m-/p-xylene, mesitylene (1,3,5-trimethylbenzene) and ethylbenzene), as well as two conjugated polycyclic ArHC (naphthalene and biphenyl). We report the elemental composition of the HOMs and show the differences in the oxidation patterns of these ArHCs. A potential pathway for the formation of these HOMs from aromatics is presented and discussed. We hypothesize that AVOC may contribute substantially to new particle formation events that have been detected in urban areas.

1 Introduction

Volatile organic compounds (VOCs) from biogenic and anthropogenic sources are the precursors of atmospheric oxidation products in the gas and particle phase. While global biogenic VOC (BVOC) emissions are a factor of 10 higher than the emissions of anthropogenic VOCs (AVOCs), the latter often dominate in the urban atmosphere (Atkinson and Arey, 2003). It was shown recently that atmospheric oxidation products of BVOCs, such as the monoterpene alpha-pinene, include highly oxygenated molecules (HOMs) through an autoxidation mechanism (Crounse et al., 2012, 2013; Ehn et al., 2014). The first step is a reaction of either OH free radicals or ozone with the VOC. After addition of O_2 to the carbon-centered radical site the $RO_2\cdot$ radical can isomerize by intra-molecular hydrogen abstraction to form a new carbon-centered radical (QOOH) (Crounse et al., 2012, 2013; Ehn et al., 2014). Further O_2-addition/isomerization sequences result in HOMs bearing several hydroperoxy groups. This autoxidation mechanism is supported by various experimental studies which used biogenic precursors, i.e. monoterpenes, sesquiterpenes, isoprene, and structural surrogates of these and computer simulations (Berndt et al., 2015; Jokinen et al., 2014, 2015; Kurtén et al., 2015; Mentel et al., 2015; Praplan et al., 2015; Richters et al., 2016;

Rissanen et al., 2014, 2015). HOMs of those compounds were found to initiate new particle formation and substantially contribute to early particle growth, which is important for the survival of newly formed particles and their ability to form cloud condensation nuclei, CCN (Bianchi et al., 2016; Kirkby et al., 2016; Tröstl et al., 2016). CCN can impact climate via their influence on cloud properties; this changes the radiation balance nowadays and did even more so in the pre-industrial period (Carslaw et al., 2013; Gordon et al., 2016).

AVOCs are comprised of a high fraction of aromatic hydrocarbons (ArHC), such as benzene, toluene, xylenes, and trimethylbenzenes, which are released from handling and combustion of fuels (Atkinson and Arey, 2003), and are important precursors for the formation of secondary organic aerosol (SOA) (Bruns et al., 2016; Li et al., 2016; Metzger et al., 2010). The OH radical is the preponderant atmospheric oxidant for ArHC except for phenols or substituted ArHC with non-aromatic double bonds where ozone and the NO_3 radical play a relevant role (Calvert et al., 2002). The addition of the OH radical to the aromatic ring results in the formation of a hydroxycyclohexadienyl-type radical (Bohn, 2001; Molina et al., 1999). Under atmospheric conditions this reacts with O_2 to yield peroxy radicals or phenolic compounds (Calvert et al., 2002; Glowacki and Pilling, 2010; Suh et al., 2003).When aromaticity is lost by OH-addition, non-aromatic double bonds are formed representing highly reactive products to more oxidants, which is a peculiar behaviour not observed in other classes of VOC (Calvert et al., 2002). This behaviour makes the investigation of ArHC oxidation more complex.

Here we show the formation of HOMs from various ArHCs upon reaction with OH radicals as has also very recently been reported by Wang et al. (2017). We present product distributions of HOMs in terms of molecular masses and molecular formulas for a series of aromatic precursors based on measurements with a nitrate chemical ionization atmospheric pressure interface time of flight mass spectrometer (CI-APi-TOF) (Ehn et al., 2014; Jokinen et al., 2012; Kürten et al., 2011). A potential pathway along with a possible mechanism for the formation of HOMs from aromatic compounds is discussed.

2 Experimental section

2.1 Flow tube

Five single-ring ArHCs: benzene (Merck, ≥ 99.7%), toluene (VWR Chemicals, ≥ 99.6%), a mixture of o-/m-/p-xylene isomers (Merck, 96%), mesitylene (1,3,5-trimethylbenzene) (Fluka, ~ 99%), ethylbenzene (Fluka, > 99%), as well as two polycyclic ArHCs naphthalene (Fluka, ≥ 99%, solid) and biphenyl (Sigma-Aldrich, ≥ 98%, solid) were investigated in a flow tube (Table 1). The experimental set-up is shown in Figure 1. Zero air from a pure air generator (Aadco Instruments, Inc., Cleves OH, USA) was used. A 104-cm long Pyrex glass tube of 7.4 cm diameter described previously (Pratte and Rossi, 2006) was used as a flow tube. Vapors of the aromatic compounds were generated from a glass vial, and collected by a stream of zero air (1.1 L min^{-1}) via a glass capillary for liquid compounds (and from a flask flushed with the same stream of zero air for solid compounds). To generate OH free radicals, zero air (7 L min^{-1}) was passed through a Nafion humidifier (Perma Pure) fed with ultra-pure water, and was then irradiated by an excimer lamp at 172 nm (7.2 eV) (Kogelschatz, 1990, 2012; Salvermoser et al., 2008). The Xe excimer lamp consists of a tubular quartz cell which surrounds a quartz flow tube

(outer diameter 10 mm) (Bartels-Rausch et al., 2011) This light photolysises O_2 and H_2O leading to the formation of OH and HO_2 radicals (see Appendix C). Subsequently, the air stream with the OH free radicals was combined at an angle of 90 degrees with the reagent flow containing the aromatic vapors before entering the flow tube, initiating the oxidation reaction. This experimental set-up avoids any potential bias due to exposure of ArHC vapors to UV radiation (Jain et al., 2012; Peng et al., 2016). This mixture (total 8.1 L min^{-1}) was injected into a laminar sheath flow of 6.7 L min^{-1} zero air at the inlet of the flow tube. The residence time in the flow tube was 20 sec. All experiments were performed at 25° C. A description of the chemical reactions involved in the excimer lamp OH radical production and a flow tube kinetic model for the mesitylene oxidation are given in Appendix C.

2.2 Instruments

The concentration of the ArHC precursors and D9-butanol as an OH tracer was measured at the exit of the flow tube with a proton-transfer-reaction time of flight mass spectrometer (PTR-TOF-MS) (Jordan et al., 2009) when the excimer lamp to generate OH free radicals was switched off and on. A nitrate chemical ionization atmospheric pressure interface time of flight mass spectrometer (CI-APi-TOF) (Ehn et al., 2014; Jokinen et al., 2012; Kürten et al., 2011) measured the chemical composition of the HOMs that were formed via OH free radical oxidation of the aromatics. HOMs were detected either through acid-base reaction or adduct formation with a nitrate ion according to the scheme:

$$HOM + NO_3^-\cdot(HNO_3)_n \rightarrow HOM\cdot\ NO_3^- + (HNO_3)_n \quad n=0\text{-}2 \quad (R1)$$
$$HOM + NO_3^-\cdot(HNO_3)_n \rightarrow HOM^- + (HNO_3)_{n+1} \quad n=0\text{-}2 \quad (R2)$$

Trifluoroacetic acid (monomer and dimer) was detected as major contaminant in the CI-APi-TOF spectra. We identified the Nafion humidifier membrane as the source of fluorinated organic compounds.

HOMs yields are calculated as the ratio of HOMs measured to ArHC reacted. HOMs were quantified using the calibration factor for sulfuric acid and assuming the same charging efficiency for HOMs (Ehn et al., 2014; Kirkby et al., 2016). From the decrease of the precursor concentration (lights off versus lights on) of D9-butanol, toluene, mesitylene and biphenyl we determined the fraction of reacted precursor. With a kinetic reaction model we then determined the initial OH concentration to be around $8.5\cdot10^{11}$ cm^{-3} (Appendix C). For the other precursors we assumed the same OH production of the lamp to calculate the fraction of reacted precursors (Table 1). Ozone, produced in the excimer irradiated region as a side product of the OH generation, was measured to be about 140 ppbv at the exit of the flow tube. It does not react with aromatic compounds. Even though some OH-oxidation products will contain a C=C double bond, the slow reaction rate of these with ozone is not expected to form significant amounts of products via this route.

3 Results and discussion

3.1 Comparison of HOMs from different ArHC

The oxidation products of the OH reaction with each of the five single-ring and two polycyclic ArHCs were measured at the exit of the tube using the CI-APi-TOF. Table 1 lists the initial concentration and the reaction rate constant of them with the OH radical, the reacted fraction (%), the HOMs concentration and the HOMs yield (%) calculated based on the reacted precursor. All investigated compounds yielded HOMs in a range between 0.1 and 2.5 % of the reacted ArHC. They were detected either as adducts with a nitrate ion (NO_3^-) or as deprotonated ions. Appendix A presents HOMs peak lists for all the ArHC compounds: for each compound we report the largest *n* peaks that sum up to 80% of the total detected signal of HOMs. Figure 2 displays the mass spectra obtained from the monocyclic aromatics. In the mass-to-charge (*m/z*) range 130 – 365 thomson (Th; 1 Th =1 Da e^{-1}, where *e* is the elementary charge), the oxidation products contain the carbon skeleton of the precursor (monomer region), while in the *m/z* range 285 – 540 Th the number of carbon atoms is doubled (dimer region). The lower end of the peak sequence (which for the benzene experiment corresponds to the oxidation product with formula $C_6H_6O_5(NO_3)^-$) is shifted by differences of 14 Th (CH_2) each from benzene via toluene and xylene/ethylbenzene to mesitylene due to the additional substituent groups. In general, a series of peaks with a mass difference of two oxygen atoms can be seen in the monomer as well as the dimer region. At each oxygen addition a few peaks are observed because oxidation compounds with the same carbon and oxygen number but different hydrogen number were observed. These peaks can be attributed to closed shell or radical compounds based on the number of hydrogen (even or odd).

HOMs from naphthalene and biphenyl are presented in Figure 3. Monomers, dimers, trimers, and tetramers are observed, and even pentamers for biphenyl. While some of the dimers may have been formed by $RO_2\cdot$ – $RO_2\cdot$ reactions, most of the higher n-mers are probably bonded by intermolecular interactions, similar to biogenic HOMs (Donahue et al., 2013). Clusters with $m/z \geq 800$ Th might already be detected by particle counters with a mobility diameter $d \geq 1.5$ nm (Kulmala et al., 2013).

In Table 2 we summarize the general features of the peak distribution of monomers, dimers and *n*-mers, as well their O:C ratios. The values given in the table cannot be considered to be absolute values, since we do not know the transmission function of the mass spectrometer. Thus, the dimer/monomer ratio might be different. However, since the mass-dependent ion transmission efficiency is rather smooth the given values may faithfully represent the relative product distribution of the different aromatic compounds. However, the given values may be a good proxy of the relative behaviour of the product distribution of the different aromatic compounds. Most of the identified peaks (77-94%) were detected as adduct with NO_3^-. The integrated signal intensity in the monomer region makes up 61 to 80% of the total detected ArHC products signal for the monocyclic ArHCs and 34-52% for the double-ring compounds. A further analysis of HOMs from monocyclic ArHC shows an increase in the dimer fraction which coincides with an increase in the methyl/ethyl substituents as follows: benzene (20%), toluene (29%), ethylbenzene (31%), xylene (35%), mesitylene (39%). This indicates that the branching ratio of $RO_2\cdot$

+ RO_2· to dimer (R3c) compared to the other reaction channels (R3a,b) is higher for the more substituted aromatics. This is based on the assumption that the lamp produces similar concentrations of OH and HO_2 radicals and that the reaction rate coefficients k(RO_2· + HO_2·) (R4a) are similar for all RO_2·. Monomers as well as dimers are highly oxygenated, even though the molecular oxygen-to-carbon (O:C) ratio is 20-30% higher for the monomers compared to the dimers. Single-ring ArHC monomers have on average an O:C ratio of 0.94 (0.50 for the double-ring ArHC) while dimers that were generated from monocyclic ArHC have on average an O:C ratio of 0.67 (0.32 for the double-ring ArHC). This may be due to the dimer formation mechanism itself, which is thought to be the formation of a peroxide C-O-O-C bond which involves elimination of molecular oxygen (Mentel et al., 2015; Wallington et al., 1992). Additionally, more oxygenated radicals have a higher probability to undergo an unimolecular termination compared to a radical-radical recombination (RO_2· + RO_2· or RO_2· + HO_2·). More oxygen atoms imply more peroxy functional groups and therefore a higher probability of a hydrogen abstraction in geminal position of a peroxide which results in an OH radical loss and a carbonyl group formation. Therefore, the fraction of dimer formation should decrease with higher oxygen content. Furthermore, we assume that less oxygenated radicals, although not quantitatively detected by the CI-APi-TOF (Berndt et al., 2015; Hyttinen et al., 2015), will nevertheless participate in the dimer formation. Substantially lower O:C ratios are found for naphthalene and biphenyl, whereby the trend between the monomers and the dimers and higher order clusters is the same as for the single-ring ArHCs. The lower O:C ratio is probably owing to the fact that the second aromatic ring remains and does not allow for extensive autoxidation.

Figure 4 shows the contribution of the most abundant identified HOMs to 80% of the total signal. The chemical composition of the observed monomers, dimers and radicals for each precursor is presented in Appendix B (Figure B-1 to Figure B-7). It is seen that in the series benzene, toluene, xylene, mesitylene the number of HOMs needed to sum up 80% of the total signal decreases (except for ethylbenzene). The increasing number of methyl groups appears to influence the oxidation pathways and leads to less HOM products. Ethylbenzene shows the highest number of HOMs. These also include monomers with 7 carbon atoms as well as dimers with an unexpectedly low number of hydrogen atoms (20 instead of 22) (Figure B – 3). This could indicate the occurrence of different pathways due to the ethyl group, a chemistry less bounded to the aromatic ring which implies an initial hydrogen abstraction step by the OH radical. Together with ethylbenzene also benzene and naphthalene, the two not substituted ArHC tested, present dimers with an unexpected low hydrogen number (12 instead of 14 and 16 instead of 18). Biphenyl also shows an unexpectedly low number of hydrogen atoms for some of the HOM monomers detected. This feature, highlighted in the four above-mentioned compounds, turns out to be a minority in terms of peaks detected and relative peak intensity.

3.2 ArHC HOMs formation mechanism

A generalized mechanism that may explain the formation of these highly oxygenated compounds from ArHCs by OH addition is exemplified for mesitylene in Figure 5. This mechanism is also applicable to the other ArHCs tested. An OH free radical attack on alkyl-substituted arenes is thought to either abstract a hydrogen atom from an sp^3 hybridized carbon, or to

add to the aromatic ring. Starting from a generic aromatic compound with formula C_xH_y, hydrogen abstraction results in a C_xH_{y-1} radical while OH addition results in a radical with the formula $C_xH_{y+1}O_1$. If we allow both initial intermediate products to proceed via autoxidation by formal addition of O_2, we expect radicals with the composition $C_xH_{y-1}O_{ze}$ (initial hydrogen abstraction) and $C_xH_{y+1}O_{zo}$ (initial OH addition) to be formed, where z denotes any number of oxygen atoms, even number (ze) in the former case and odd number (zo) in the latter case. This addition of molecular O_2 increases the mass of the compounds by 32 Da resulting in the propagation of a radical with an odd number of oxygen atoms. This can be seen by *m/z* shifts of 32 Th in the mass spectra. For the ArHCs tested we do not observe radicals with the formula $C_xH_{y-1}O_{ze}$, owing to the fact that hydrogen abstraction is a minor pathway (with e.g. a branching ratio of 7% for toluene according to the Master Chemical Mechanism MCM 3.3.1 (Jenkin et al., 2003), which yields products like benzaldehyde and benzyl alcohol). For mesitylene (Figure 5), the OH-adduct and the first $RO_2\cdot$ radical ($HO\text{-}C_xH_yOO\cdot$) cannot be detected with the nitrate CI-APi-TOF (Hyttinen et al., 2015) and are reported in grey in Figure 5. More highly oxygenated $RO_2\cdot$ radicals with the formula $C_9H_{13}O_{5\text{-}11}$ were however found, with the highest intensity for $C_9H_{13}O_7$ (3% of the sum of the identified HOMs). In addition to radicals with an odd oxygen number, radicals with an even oxygen number of molecular formula $C_xH_{y+1}O_{ze}$ were observed (Figure 5). These radicals are likely produced via $RO_2\cdot + RO_2\cdot$ (or $RO_2\cdot + HO_2\cdot$), involving the formation of an alkoxy radical intermediate (Lightfoot et al., 1992; Mentel et al., 2015; Orlando and Tyndall, 2012; Vereecken and Peeters, 2009) according to:

$$\begin{aligned}
ROO\cdot + R'OO\cdot &\rightarrow RO\cdot + R'O\cdot + O_2 && \text{(R3a)}\\
&\rightarrow ROH + R'_{\text{-H}}O + O_2 && \text{(R3b)}\\
&\rightarrow ROOR' + O_2 && \text{(R3c)}\\
ROO\cdot + HOO\cdot &\rightarrow ROOH + O_2 && \text{(R4a)}\\
&\rightarrow RO\cdot + \cdot OH + O_2 && \text{(R4b)}
\end{aligned}$$

These alkoxy radicals (R3a and R4b) may isomerize to an alcohol by internal H-abstraction forming a carbon centred radical, which can again take up an oxygen molecule and follow the autoxidation route. The peroxy radicals of this reaction channel have the formula $C_xH_{y+1}O_{ze}$ (see Fig.5). Besides the formation of alkoxy radicals recombination can also lead to a carbonyl and alcohol species (R3b) with the formulae $C_xH_yO_z$ and $C_xH_{y+2}O_z$. The much higher intensity of the peaks with formula $C_xH_{y+2}O_z$ compared to those with the composition $C_xH_yO_z$ can be ascribed to a high contribution from the recombination of $RO_2\cdot$ with $HO_2\cdot$ (R4a). This is due to the high $HO_2\cdot$ concentration in our experiments since $HO_2\cdot$ is also formed in the OH radical source. The formation of ROOR (R3c) corresponds to $C_{2x}H_{2y+2}O_z$ dimer formation with z being even or odd, depending on the combination of the reacting peroxy radicals. We also detected free radicals and closed-shell molecules with an unexpectedly high number of hydrogen atoms, with the formulae $C_xH_{y+(3,5)}O_z$ and $C_xH_{y+(4,6)}O_z$, respectively. For mesitylene (Fig. 5), radicals with the formula $C_9H_{15}O_{7\text{-}11}$ were identified, with the highest signals found for $C_9H_{15}O_7$ (1%), and $C_9H_{15}O_8$ (2%). These compounds are likely formed by a second OH addition as discussed further below. Monomer closed-shell molecules were detected as $C_9H_{12}O_{5\text{-}11}$ (4%), $C_9H_{14}O_{4\text{-}11}$ (25%), and $C_9H_{16}O_{5\text{-}10}$ (12%). We assume that the

$C_9H_{12}O_{5\text{-}11}$ molecules derive from the first radical generation ($C_9H_{13}O_{5\text{-}11}$) and the $C_9H_{16}O_{5\text{-}10}$ molecules from a second OH attack ($C_9H_{15}O_{7\text{-}11}$). The $C_9H_{14}O_{4\text{-}11}$ molecules may be produced from either the first or the second OH attack. However further investigation is required to test these hypotheses. We also want to point out that the relative signal intensities may be biased by the nitrate clustering properties and do not necessarily reflect the actual distribution of compounds. Similarly, the compounds with an H-atom number lower than the ArHC precursor could have been formed by an H-abstraction from first generation products with formula $C_xH_yO_z$.

The recombination of two peroxy radicals may lead to a covalently-bound peroxy-bridged dimer. We observed three classes of such products (Figure 5): i) from the recombination of two first-generation radicals (13 hydrogen atoms each) with the molecular formula $C_{18}H_{26}O_{8\text{-}13}$ (30% of the total intensity), ii) from the recombination of a first generation radical with a second generation radical (13 + 15 hydrogen atoms) with formula $C_{18}H_{28}O_{9\text{-}12}$ (3% of the total signal), and iii) from the recombination of two radicals from the second generation (15 + 15 hydrogen atoms), where only one compound was identified ($C_{18}H_{30}O_{11}$, 1%).

Some identified monomer and dimer peaks belong to oxygenated molecules with less carbon atoms than the respective precursor. This is likely the result of a fragmentation process. HOMs with less C atoms than the parent molecule have also been previously described from terpene precursors via CO elimination (Rissanen et al., 2014, 2015). Here, the aromatics show mostly also a loss of H-atoms when fragmenting. This indicates that a methyl group can be lost after oxidation to an alkoxy radical as formaldehyde or a carbon fragment can be lost after ring cleavage. As mentioned above, we hypothesize that the $C_xH_{y+(3,5)}O_z$ radicals and $C_xH_{y+(4,6)}O_z$ molecules may have formed by multiple OH attacks in our reactor. This is possible when the second OH attacks a product molecule that contains two hydrogen atoms more than the parent molecule. To allow for the addition of a second OH free radical these first generation closed-shell molecules must still contain a carbon-carbon double bond in their structure. A third OH attack is observed only for some compounds: benzene, ethylbenzene, xylene, naphthalene and biphenyl; the contribution of these HOMs to the total of the detected signals is always extremely low. The mechanism will likely proceed in a similar way.

An explicit mechanism after OH addition for a possible pathway of the aromatic autoxidation is suggested in Figure 6 for up to seven oxygen atoms. After addition of OH and loss of aromaticity an oxygen molecule can be added forming a peroxy radical. It has been established that the latter can cyclize producing a second stabilized allylic radical with an endocyclic O_2 bridge (Baltaretu et al., 2009; Birdsall and Elrod, 2011; Pan and Wang, 2014). To this oxygen bridged bicyclic radical further oxygen additions followed by cyclization or internal H-abstraction might occur up to a peroxy radical with seven oxygen atoms ($C_9H_{13}O_7$), which is the species detected at relatively high intensity (3.5%). Two potential routes are shown in Figure 6. One follows the traditional autoxidation mechanism with internal H-abstraction and oxygen addition (Type I autoxidation). The other route proposes another cyclization forming a second oxygen bridge. This mechanism also produces a carbon centered radical and promotes autoxidation (Type II) by the addition of another oxygen molecule. Wang et al. (2017) provide evidence from isotope labelling experiments for the occurrence of Type I autoxidation in isopropylbenzene. Some of the ArHC tested also form radicals with a higher number of odd oxygens (i.e., up to 9-11 O atoms, Appendix B)

indicating that autoxidation may even proceed further. Compounds with an even number of oxygen are formed via the alkoxy pathway and may also include a ring opening step. Possible branching channels where this may happen are indicated in Figure 6. Termination reactions to alcohols (R3b) or hydroperoxides (R4a) can form molecules still containing double bonds which can further add an OH radical leading to compounds with four hydrogen atoms more than the precursor.

As mentioned above naphthalene and biphenyl, despite the polycyclic skeleton, do not show a radically different behaviour compared to the single-ring ArHCs. The maximum number of oxygen atoms that their monomer HOMs can host is 10 for naphthalene and 11 for biphenyl. Biphenyl seems to compare with its single ring analogue benzene. $C_6H_8O_5$ and $C_{12}H_{12}O_5$ are the strongest peaks indicating that the oxidation of one benzene ring in biphenyl proceeds in a similar way. Similarly, the strongest dimer is $C_{12}H_{14}O_8$ for benzene and $C_{24}H_{22}O_8$ for biphenyl, respectively. Compounds with extra-high H-atoms are more frequently found for biphenyl, which is expected as there is a second reactive aromatic ring remaining after (auto)-oxidation of the first one. Thus, a second OH attack is probable. Naphthalene seems to take up less oxygen than the other compounds, showing the maximum signal intensity at 4-5 oxygen atoms for monomers and only 4-6 for dimers. This may indicate that not both rings can easily be autoxidized in one step. It is also interesting to note that compounds from a second OH attack do not show a strong increase of the oxygen content, neither for the single nor for the double ring ArHCs.

4 Conclusions and atmospheric implications

All tested compounds yielded HOMs and we conclude that this is a common feature of aromatic compounds. Similar to the oxidation process that yields HOMs from terpenes the oxidation process of ArHC yields highly oxygenated compounds containing the carbon skeleton of the precursor (monomers) as well as twice as many carbons (dimers). It is known from previous studies that ArHC are able to add molecular oxygen to the molecule after OH addition forming an oxygen-bridged bicyclic radical. Our measurements of highly oxygenated compounds up to eleven oxygen atoms in a monomer reveal that an autoxidation radical chain reaction occurs by adding several more oxygens to the initially formed radical. The autoxidation radical chain reaction is thought to proceed via intra-molecular abstraction of a hydrogen atom from an acidic C-H bond by a peroxy radical and the consequent formation of a hydroperoxy functional group and a carbon centered radical that can take up an oxygen molecule from the surrounding and eventually repeat the whole process n times (Type I autoxidation). In the case of aromatic compounds, when the aromaticity is destroyed, Type II autoxidation may happen by further addition of oxygen to the allylic resonance-stabilized radical followed by an attack of the peroxy group to the internal double bonds forming an oxygen bridge. This can proceed up to a peroxy radical of 7 oxygen. Type II autoxidation has also been proposed to occur with sesquiterpenes with two double bonds(Richters et al., 2016) and also with α-pinene for certain HOMs (Rissanen et al., 2015). Even though the autoxidation of ArHCs will lead to different chemical compounds compared to HOMs form terpenes we expect similar chemical and physical characteristics such as functional groups and volatility. In both cases extremely low volatility highly oxygenated dimer species are formed, which may play an important role in new particle formation.

Recent studies (Nakao et al., 2011; Schwantes et al., 2017) suggest that from hydroxy ArHC equivalents, which are formed in the first generation OH oxidation of aromatics, additional OH oxidation steps can produce substantial amounts of polyhydroxy aromatics with high O:C ratio (up to 1.2). However literature data are showing varying yields for the conversion of arenes to phenols via the OH radical addition and H elimination. According to MCM 3.3.1 (Jenkin et al., 2003) benzene and toluene have quite high phenol yields (approximately 50 and 20 %, respectively) while mesitylene shows a rather small yield (4%). This fact should be reflected in the final HOMs yield with alkyl substituted ArHCs being less effective in yielding HOMs. However in our experiments we did not detect such a difference in the HOMs yields linked to phenol formation yields. A relevant fraction of the detected HOMs showed a hydrogen atom number higher than the precursor ArHC which cannot be explained with the presence of just polyphenolic compounds as oxidation products.

Quantum chemical calculations have revealed that intramolecular H-migrations in bicyclic peroxy radicals may be a feasible route to HOMs (Wang et al., 2017). Especially aromatics with a longer chain substituent (ethyl-, isopropylbenzene) or multiple substituents may have a fast HOM formation pathway. Indeed our measurements show somewhat higher HOM yields for xylene and mesitylene compared to benzene and toluene. However more kinetic and mechanistic studies are needed to better understand HOM formation from the various aromatics.

Under urban conditions, in the presence of NO, the reaction of $RO_2\cdot$ + NO will compete with the autoxidation pathway. This can lead to relatively highly oxygenated nitrates of low volatility or oxyradicals. The latter can isomerize to a carbon centred radical as under our conditions and again undergo autoxidation. Highly oxygenated organic nitrates have been recently identified in SOA (Lee et al., 2016). While this study shows that autoxidation can also occur after an OH attack of ArHC, the formation of low volatility products via this route in the presence of NO, which is typical of urban atmospheres, needs further investigation. Furthermore, first generation oxidation products may still contain carbon-carbon double bonds, which could also further react with ozone forming more highly oxygenated products. Since the reaction time is very short in the flow tube this reaction is negligible but could be another potential pathway in the ambient atmosphere.

Some of the HOMs measured here from the oxidation of ArHC have the same composition as the HOMs formulae identified by Bianchi et al. (2016) during winter time nucleation episodes at the Jungfraujoch High Altitude Research Station.

The fact that the oxidation of ArHC can rapidly form HOMs of very low volatility makes ArHC a potential contributor to nucleation and early particle growth during nucleation episodes observed in urban areas. (Stanier et al., 2004; Wang et al., 2015; Xiao et al., 2015; Yu et al., 2016).

Acknowledgments.

We thank Prof. Dr. Markus Ammann for the laboratory equipment, Dr. Dogushan Kilic for technical support, Dr. Simone Maria Pieber and Dr. Christopher Robert Hoyle for scientific discussions and comments on the manuscript. The tofTools team is acknowledged for providing tools for mass spectrometry analysis. This work was supported by the Swiss National Science Foundation (20020_152907 / 1).

References

Atkinson, R. and Arey, J.: Atmospheric degradation of volatile organic compounds, Chem. Rev., 103(12), 4605–4638, doi:10.1021/cr0206420, 2003.

Baltaretu, C. O., Lichtman, E. I., Hadler, A. B. and Elrod, M. J.: Primary atmospheric oxidation mechanism for toluene, J. Phys. Chem. A, 113(1), 221–230, doi:10.1021/jp806841t, 2009.

Bartels-Rausch, T., Ulrich, T., Huthwelker, T. and Ammann, M.: A novel synthesis of the N-13 labeled atmospheric trace gas peroxynitric acid, Radiochim. Acta, 99(5), 285–292, doi:10.1524/ract.2011.1830, 2011.

Berndt, T., Richters, S., Kaethner, R., Voigtländer, J., Stratmann, F., Sipilä, M., Kulmala, M. and Herrmann, H.: Gas-phase ozonolysis of cycloalkenes: formation of highly oxidized RO_2 radicals and their reactions with NO, NO_2, SO_2 and other RO_2 radicals, J. Phys. Chem. A, (2), 150923134432004, doi:10.1021/acs.jpca.5b07295, 2015.

Bianchi, F., Trostl, J., Junninen, H., Frege, C., Henne, S., Hoyle, C. R., Molteni, U., Herrmann, E., Adamov, A., Bukowiecki, N., Chen, X., Duplissy, J., Gysel, M., Hutterli, M., Kangasluoma, J., Kontkanen, J., Kurten, A., Manninen, H. E., Munch, S., Perakyla, O., Petaja, T., Rondo, L., Williamson, C., Weingartner, E., Curtius, J., Worsnop, D. R., Kulmala, M., Dommen, J. and Baltensperger, U.: New particle formation in the free troposphere: A question of chemistry and timing, Science, 352(6289), 1109–1112, doi:10.1126/science.aad5456, 2016.

Birdsall, A. W. and Elrod, M. J.: Comprehensive NO-dependent study of the products of the oxidation of atmospherically relevant aromatic compounds, J. Phys. Chem. A, 115(21), 5397–5407, doi:10.1021/jp2010327, 2011.

Bohn, B.: Formation of peroxy radicals from OH−toluene adducts and O_2, J. Phys. Chem. A, 105(25), 6092–6101, doi:10.1021/jp0033972, 2001.

Bruns, E. A., El Haddad, I., Slowik, J. G., Kilic, D., Klein, F., Baltensperger, U. and Prévôt, A. S. H.: Identification of significant precursor gases of secondary organic aerosols from residential wood combustion, Sci. Rep., 6 (February), 27881, doi:10.1038/srep27881, 2016.

Calvert, J. G., Atkinson, R., Becker, K. H., Kamens, R. M., Seinfeld, J. H., Wallington, T. H. and Yarwood, G.: The mechanisms of atmospheric oxidation of the aromatic hydrocarbons, Oxford University Press., 2002.

Carslaw, K. S., Lee, L. a, Reddington, C. L., Pringle, K. J., Rap, A., Forster, P. M., Mann, G. W., Spracklen, D. V, Woodhouse, M. T., Regayre, L. and Pierce, J. R.: Large contribution of natural aerosols to uncertainty in indirect forcing, Nature, 503(7474), 67–71, doi:10.1038/nature12674, 2013.

Crounse, J. D., Knap, H. C., Ørnsø, K. B., Jørgensen, S., Paulot, F., Kjaergaard, H. G. and Wennberg, P. O.: Atmospheric fate of methacrolein. 1. peroxy radical isomerization following addition of OH and O_2, J. Phys. Chem. A, 116(24), 5756–5762, doi:10.1021/jp211560u, 2012.

Crounse, J. D., Nielsen, L. B., Jørgensen, S., Kjaergaard, H. G. and Wennberg, P. O.: Autoxidation of organic compounds in the atmosphere, J. Phys. Chem. Lett., 4(20), 3513–3520, doi:10.1021/jz4019207, 2013.

Donahue, N. M., Ortega, I. K., Chuang, W., Riipinen, I., Riccobono, F., Schobesberger, S., Dommen, J., Baltensperger, U., Kulmala, M., Worsnop, D. R. and Vehkamaki, H.: How do organic vapors contribute to new-particle formation?, Faraday Discuss., 165, 91, doi:10.1039/c3fd00046j, 2013.

Ehn, M., Thornton, J. a., Kleist, E., Sipilä, M., Junninen, H., Pullinen, I., Springer, M., Rubach, F., Tillmann, R., Lee, B., Lopez-Hilfiker, F., Andres, S., Acir, I.-H., Rissanen, M., Jokinen, T., Schobesberger, S., Kangasluoma, J., Kontkanen, J., Nieminen, T., Kurtén, T., Nielsen, L. B., Jørgensen, S., Kjaergaard, H. G., Canagaratna, M., Maso, M. D., Berndt, T., Petäjä, T., Wahner, A., Kerminen, V.-M., Kulmala, M., Worsnop, D. R., Wildt, J. and Mentel, T. F.: A large source of low-volatility secondary organic aerosol, Nature, 506(7489), 476–479, doi:10.1038/nature13032, 2014.

Glowacki, D. R. and Pilling, M. J.: Unimolecular reactions of peroxy radicals in atmospheric chemistry and combustion, ChemPhysChem, 11(18), 3836–3843, doi:10.1002/cphc.201000469, 2010.

Gordon, H., Sengupta, K., Rap, A., Duplissy, J., Frege, C., Williamson, C., Heinritzi, M., Simon, M., Yan, C., Almeida, J., Tröstl, J., Nieminen, T., Ortega, I. K., Wagner, R., Dunne, E. M., Adamov, A., Amorim, A., Bernhammer, A.-K., Bianchi, F., Breitenlechner, M., Brilke, S., Chen, X., Craven, J. S., Dias, A., Ehrhart, S., Fischer, L., Flagan, R. C., Franchin, A., Fuchs, C., Guida, R., Hakala, J., Hoyle, C. R., Jokinen, T., Junninen, H., Kangasluoma, J., Kim, J., Kirkby, J., Krapf, M., Kürten, A., Laaksonen, A., Lehtipalo, K., Makhmutov, V., Mathot, S., Molteni, U., Monks, S. A., Onnela, A., Peräkylä, O., Piel, F., Petäjä, T., Praplan, A. P., Pringle, K. J., Richards, N. A. D., Rissanen, M. P., Rondo, L., Sarnela, N., Schobesberger, S., Scott, C. E., Seinfeld, J. H., Sharma, S., Sipilä, M., Steiner, G., Stozhkov, Y., Stratmann, F., Tomé, A., Virtanen, A., Vogel, A. L., Wagner, A. C., Wagner, P. E., Weingartner, E., Wimmer, D., Winkler, P. M., Ye, P., Zhang, X., Hansel, A., Dommen, J., Donahue, N. M., Worsnop, D. R., Baltensperger, U., Kulmala, M., Curtius, J. and Carslaw, K. S.: Reduced anthropogenic aerosol radiative forcing caused by biogenic new particle formation, Proc. Natl. Acad. Sci., 201602360, doi:10.1073/pnas.1602360113, 2016.

Hyttinen, N., Kupiainen-Määttä, O., Rissanen, M. P., Muuronen, M., Ehn, M. and Kurtén, T.: Modeling the charging of highly oxidized cyclohexene ozonolysis products using nitrate-based chemical ionization, J. Phys. Chem. A, 119(24), 6339–6345, doi:10.1021/acs.jpca.5b01818, 2015.

Jain, C., Morajkar, P., Schoemaecker, C. and Fittschen, C.: Formation of HO_2 radicals from the 248 nm two-photon excitation of different aromatic hydrocarbons in the presence of O_2, J. Phys. Chem. A, 116(24), 6231–6239, doi:10.1021/jp211520g, 2012.

Jenkin, M. E., Saunders, S. M., Wagner, V. and Pilling, M. J.: Protocol for the development of the Master Chemical Mechanism, MCM v3 (Part B): tropospheric degradation of aromatic volatile organic compounds, Atmos. Chem. Phys., 3(1), 181–193, doi:10.5194/acp-3-181-2003, 2003.

Jokinen, T., Sipilä, M., Junninen, H., Ehn, M., Lönn, G., Hakala, J., Petäjä, T., Mauldin, R. L., Kulmala, M. and Worsnop, D. R.: Atmospheric sulphuric acid and neutral cluster measurements using CI-APi-TOF, Atmos. Chem. Phys., 12(9), 4117–4125, doi:10.5194/acp-12-4117-2012, 2012.

Jokinen, T., Sipilä, M., Richters, S., Kerminen, V.-M., Paasonen, P., Stratmann, F., Worsnop, D., Kulmala, M., Ehn, M., Herrmann, H. and Berndt, T.: Rapid autoxidation forms highly oxidized RO_2 radicals in the atmosphere, Angew. Chemie Int. Ed., 53(52), 14596–14600, doi:10.1002/anie.201408566, 2014.

Jokinen, T., Berndt, T., Makkonen, R., Kerminen, V., Junninen, H., Paasonen, P., Stratmann, F., Herrmann, H., Guenther, A. B., Worsnop, D. R., Kulmala, M., Ehn, M. and Sipilä, M.: Production of extremely low volatile organic compounds from biogenic emissions: Measured yields and atmospheric implications, Proc. Natl. Acad. Sci., 112(23), 7123–7128, doi:10.1073/pnas.1423977112, 2015.

Jordan, A., Haidacher, S., Hanel, G., Hartungen, E., Märk, L., Seehauser, H., Schottkowsky, R., Sulzer, P. and Märk, T. D.: A high resolution and high sensitivity proton-transfer-reaction time-of-flight mass spectrometer (PTR-TOF-MS), Int. J. Mass Spectrom., 286(2–3), 122–128, doi:10.1016/j.ijms.2009.07.005, 2009.

Kirkby, J., Duplissy, J., Sengupta, K., Frege, C., Gordon, H., Williamson, C., Heinritzi, M., Simon, M., Yan, C., Almeida, J., Tröstl, J., Nieminen, T., Ortega, I. K., Wagner, R., Adamov, A., Amorim, A., Bernhammer, A.-K., Bianchi, F., Breitenlechner, M., Brilke, S., Chen, X., Craven, J., Dias, A., Ehrhart, S., Flagan, R. C., Franchin, A., Fuchs, C., Guida, R., Hakala, J., Hoyle, C. R., Jokinen, T., Junninen, H., Kangasluoma, J., Kim, J., Krapf, M., Kürten, A., Laaksonen, A., Lehtipalo, K., Makhmutov, V., Mathot, S., Molteni, U., Onnela, A., Peräkylä, O., Piel, F., Petäjä, T., Praplan, A. P., Pringle, K., Rap, A., Richards, N. A. D., Riipinen, I., Rissanen, M. P., Rondo, L., Sarnela, N., Schobesberger, S., Scott, C. E., Seinfeld, J. H., Sipilä, M., Steiner, G., Stozhkov, Y., Stratmann, F., Tomé, A., Virtanen, A., Vogel, A. L., Wagner, A. C., Wagner, P. E., Weingartner, E., Wimmer, D., Winkler, P. M., Ye, P., Zhang, X., Hansel, A., Dommen, J., Donahue, N. M., Worsnop, D. R., Baltensperger, U., Kulmala, M., Carslaw, K. S. and Curtius, J.: Ion-induced nucleation of pure biogenic particles, Nature, 533(7604), 521–526, doi:10.1038/nature17953, 2016.

Kogelschatz, U.: Silent discharges for the generation of ultraviolet and vacuum ultraviolet excimer radiation, Pure Appl. Chem., 62(9), 1667–1674, doi:10.1351/pac199062091667, 1990.

Kogelschatz, U.: Ultraviolet excimer radiation from nonequilibrium gas discharges and its application in photophysics, photochemistry and photobiology, J. Opt. Technol., 79(8), 484, doi:10.1364/JOT.79.000484, 2012.

Kulmala, M., Kontkanen, J., Junninen, H., Lehtipalo, K., Manninen, H. E., Nieminen, T., Petaja, T., Sipila, M., Schobesberger, S., Rantala, P., Franchin, A., Jokinen, T., Jarvinen, E., Aijala, M., Kangasluoma, J., Hakala, J., Aalto, P. P., Paasonen, P., Mikkila, J., Vanhanen, J., Aalto, J., Hakola, H., Makkonen, U., Ruuskanen, T., Mauldin, R. L., Duplissy, J., Vehkamaki, H., Back, J., Kortelainen, A., Riipinen, I., Kurten, T., Johnston, M. V, Smith, J. N., Ehn, M., Mentel, T. F., Lehtinen, K. E. J., Laaksonen, A., Kerminen, V.-M. and Worsnop, D. R.: Direct observations of atmospheric aerosol nucleation, Science, 339(6122), 943–946, doi:10.1126/science.1227385, 2013.

Kürten, A., Rondo, L., Ehrhart, S. and Curtius, J.: Performance of a corona ion source for measurement of sulfuric acid by chemical ionization mass spectrometry, Atmos. Meas. Tech., 4, 437–443, doi:10.5194/amt-4-437-2011, 2011.

Kurtén, T., Rissanen, M. P., Mackeprang, K., Thornton, J. A., Hyttinen, N., Jørgensen, S., Ehn, M. and Kjaergaard, H. G.: Computational study of hydrogen shifts and ring-opening mechanisms in α-pinene ozonolysis products, J. Phys. Chem. A, 119(46), 11366–11375, doi:10.1021/acs.jpca.5b08948, 2015.

Lee, B. H., Mohr, C., Lopez-Hilfiker, F. D., Lutz, A., Hallquist, M., Lee, L., Romer, P., Cohen, R. C., Iyer, S., Kurtén, T., Hu, W., Day, D. A., Campuzano-Jost, P., Jimenez, J. L., Xu, L., Ng, N. L., Guo, H., Weber, R. J., Wild, R. J., Brown, S. S., Koss, A., de Gouw, J., Olson, K., Goldstein, A. H., Seco, R., Kim, S., McAvey, K., Shepson, P. B., Starn, T., Baumann, K., Edgerton, E. S., Liu, J., Shilling, J. E., Miller, D. O., Brune, W., Schobesberger, S., D'Ambro, E. L. and Thornton, J. A.: Highly functionalized organic nitrates in the southeast United States: Contribution to secondary organic aerosol and reactive nitrogen budgets, Proc. Natl. Acad. Sci., 113(6), 1516–1521, doi:10.1073/pnas.1508108113, 2016.

Li, L., Tang, P., Nakao, S., Kacarab, M. and Cocker, D. R.: Novel approach for evaluating secondary organic aerosol from aromatic hydrocarbons: unified method for predicting aerosol composition and formation, Environ. Sci. Technol., 50(12), 6249–6256, doi:10.1021/acs.est.5b05778, 2016.

Lightfoot, P., Cox, R., Crowley, J., Destriau, M., Hayman, G., Jenkin, M., Moortgat, G. and Zabel, F.: Organic peroxy radicals: kinetics, spectroscopy and tropospheric chemistry, Atmos. Environ. Part A. Gen. Top., 26(10), 1805–1961, doi:10.1016/0960-1686(92)90423-I, 1992.

Mentel, T. F., Springer, M., Ehn, M., Kleist, E., Pullinen, I., Kurtén, T., Rissanen, M., Wahner, A. and Wildt, J.: Formation of highly oxidized multifunctional compounds: autoxidation of peroxy radicals formed in the ozonolysis of alkenes – deduced from structure – product relationships, Atmos. Chem. Phys., 15(12), 6745–6765, doi:10.5194/acp-15-6745-2015, 2015.

Metzger, A., Verheggen, B., Dommen, J., Duplissy, J., Prevot, A. S. H., Weingartner, E., Riipinen, I., Kulmala, M., Spracklen, D. V, Carslaw, K. S. and Baltensperger, U.: Evidence for the role of organics in aerosol particle formation under atmospheric conditions, Proc. Natl. Acad. Sci., 107(15), 6646–6651, doi:10.1073/pnas.0911330107, 2010.

Molina, M. J., Zhang, R., Broekhuizen, K., Lei, W., Navarro, R. and Molina, L. T.: Experimental study of intermediates from OH-initiated reactions of toluene, J. Am. Chem. Soc., 121(43), 10225–10226, doi:10.1021/ja992461u, 1999.

Nakao, S., Clark, C., Tang, P., Sato, K. and Cocker, D.: Secondary organic aerosol formation from phenolic compounds in the absence of NOx, Atmos. Chem. Phys., 11(20), 10649–10660, doi:10.5194/acp-11-10649-2011, 2011.

Orlando, J. J. and Tyndall, G. S.: Laboratory studies of organic peroxy radical chemistry: an overview with emphasis on recent issues of atmospheric significance, Chem. Soc. Rev., 41(19), 6294, doi:10.1039/c2cs35166h, 2012.

Pan, S. and Wang, L.: Atmospheric oxidation mechanism of m-Xylene initiated by OH radical, J. Phys. Chem. A, 118(45), 10778–10787, doi:10.1021/jp506815v, 2014.

Peng, Z., Day, D. A., Ortega, A. M., Palm, B. B., Hu, W., Stark, H., Li, R., Tsigaridis, K., Brune, W. H. and Jimenez, J. L.: Non-OH chemistry in oxidation flow reactors for the study of atmospheric chemistry systematically examined by modeling, Atmos. Chem. Phys., 16(7), 4283–4305, doi:10.5194/acp-16-4283-2016, 2016.

Praplan, a. P., Schobesberger, S., Bianchi, F., Rissanen, M. P., Ehn, M., Jokinen, T., Junninen, H., Adamov, A., Amorim, A., Dommen, J., Duplissy, J., Hakala, J., Hansel, A., Heinritzi, M., Kangasluoma, J., Kirkby, J., Krapf, M., Kürten, A., Lehtipalo, K., Riccobono, F., Rondo, L., Sarnela, N., Simon, M., Tomé, A., Tröstl, J., Winkler, P. M., Williamson, C., Ye, P., Curtius, J., Baltensperger, U., Donahue, N. M., Kulmala, M. and Worsnop, D. R.: Elemental composition and clustering behaviour of α-pinene oxidation products for different oxidation conditions, Atmos. Chem. Phys., 15(8), 4145–4159, doi:10.5194/acp-15-4145-2015, 2015.

Pratte, P. and Rossi, M. J.: The heterogeneous kinetics of HOBr and HOCl on acidified sea salt and model aerosol at 40–90% relative humidity and ambient temperature, Phys. Chem. Chem. Phys., 8(34), 3988–4001, doi:10.1039/B604321F, 2006.

Richters, S., Herrmann, H. and Berndt, T.: Highly oxidized RO_2 radicals and consecutive products from the ozonolysis of three sesquiterpenes, Environ. Sci. Technol., 50(5), 2354–2362, doi:10.1021/acs.est.5b05321, 2016.

Rissanen, M. P., Kurtén, T., Sipilä, M., Thornton, J. A., Kangasluoma, J., Sarnela, N., Junninen, H., Jørgensen, S., Schallhart, S., Kajos, M. K., Taipale, R., Springer, M., Mentel, T. F., Ruuskanen, T., Petäjä, T., Worsnop, D. R., Kjaergaard, H. G. and

Ehn, M.: The formation of highly oxidized multifunctional products in the ozonolysis of cyclohexene, J. Am. Chem. Soc., 136(44), 15596–15606, doi:10.1021/ja507146s, 2014.

Rissanen, M. P., Kurtén, T., Sipilä, M., Thornton, J. a., Kausiala, O., Garmash, O., Kjaergaard, H. G., Petäjä, T., Worsnop, D. R., Ehn, M. and Kulmala, M.: Effects of chemical complexity on the autoxidation mechanisms of endocyclic alkene ozonolysis products: from methylcyclohexenes toward understanding α-pinene, J. Phys. Chem. A, 119(19), 4633–4650, doi:10.1021/jp510966g, 2015.

Salvermoser, M., Murnick, D. E. and Kogelschatz, U.: Influence of water vapor on photochemical ozone generation with efficient 172 nm xenon excimer lamps, Ozone Sci. Eng., 30(3), 228–237, doi:10.1080/01919510802070611, 2008.

Schwantes, R. H., Schilling, K. A., McVay, R. C., Lignell, H., Coggon, M. M., Zhang, X., Wennberg, P. O. and Seinfeld, J. H.: Formation of highly oxygenated low-volatility products from cresol oxidation, Atmos. Chem. Phys., 17, 3453–3474, doi:10.5194/acp-17-3453-2017.

Stanier, C. O., Khlystov, A. Y. and Pandis, S. N.: Nucleation events during the Pittsburgh air quality study: description and relation to key meteorological, gas phase, and aerosol parameters. Special Issue of Aerosol Science and Technology on Findings from the Fine Particulate Matter Supersites Program, Aerosol Sci. Technol., 38(sup1), 253–264, doi:10.1080/02786820390229570, 2004.

Suh, I., Zhang, R., Molina, L. T. and Molina, M. J.: Oxidation mechanism of aromatic peroxy and bicyclic radicals from OH−toluene reactions, J. Am. Chem. Soc., 125(41), 12655–12665, doi:10.1021/ja0350280, 2003.

Tröstl, J., Chuang, W. K., Gordon, H., Heinritzi, M., Yan, C., Molteni, U., Ahlm, L., Frege, C., Bianchi, F., Wagner, R., Simon, M., Lehtipalo, K., Williamson, C., Craven, J. S., Duplissy, J., Adamov, A., Almeida, J., Bernhammer, A.-K., Breitenlechner, M., Brilke, S., Dias, A., Ehrhart, S., Flagan, R. C., Franchin, A., Fuchs, C., Guida, R., Gysel, M., Hansel, A., Hoyle, C. R., Jokinen, T., Junninen, H., Kangasluoma, J., Keskinen, H., Kim, J., Krapf, M., Kürten, A., Laaksonen, A., Lawler, M., Leiminger, M., Mathot, S., Möhler, O., Nieminen, T., Onnela, A., Petäjä, T., Piel, F. M., Miettinen, P., Rissanen, M. P., Rondo, L., Sarnela, N., Schobesberger, S., Sengupta, K., Sipilä, M., Smith, J. N., Steiner, G., Tomè, A., Virtanen, A., Wagner, A. C., Weingartner, E., Wimmer, D., Winkler, P. M., Ye, P., Carslaw, K. S., Curtius, J., Dommen, J., Kirkby, J., Kulmala, M., Riipinen, I., Worsnop, D. R., Donahue, N. M. and Baltensperger, U.: The role of low-volatility organic compounds in initial particle growth in the atmosphere, Nature, 533(7604), 527–531, doi:10.1038/nature18271, 2016.

Vereecken, L. and Peeters, J.: Decomposition of substituted alkoxy radicals-part I: a generalized structure-activity relationship for reaction barrier heights., Phys. Chem. Chem. Phys., 11(40), 9062–9074, doi:10.1039/b909712k, 2009.

Wallington, T. J., Dagaut, P. and Kurylo, M. J.: UV absorption cross sections and reaction kinetics and mechanisms for peroxy radicals in the gas phase, Chem. Rev., 92(4), 667–710, doi:10.1021/cr00012a008, 1992.

Wang, S., Wu, R., Berndt, T., Ehn, M. and Wang, L.: Formation of highly oxidized radicals and multifunctional products from the atmospheric oxidation of alkylbenzenes, Environ. Sci. Technol., 51(15), 8442–8449, doi:10.1021/acs.est.7b02374, 2017.

Wang, Z. B., Hu, M., Pei, X. Y., Zhang, R. Y., Paasonen, P., Zheng, J., Yue, D. L., Wu, Z. J., Boy, M. and Wiedensohler, A.: Connection of organics to atmospheric new particle formation and growth at an urban site of Beijing, Atmos. Environ., 103, 7–17, doi:10.1016/j.atmosenv.2014.11.069, 2015.

Xiao, S., Wang, M. Y., Yao, L., Kulmala, M., Zhou, B., Yang, X., Chen, J. M., Wang, D. F., Fu, Q. Y., Worsnop, D. R. and Wang, L.: Strong atmospheric new particle formation in winter in urban Shanghai, China, Atmos. Chem. Phys., 15(4), 1769–1781, doi:10.5194/acp-15-1769-2015, 2015.

Yu, H., Zhou, L., Dai, L., Shen, W., Dai, W., Zheng, J., Ma, Y. and Chen, M.: Nucleation and growth of sub-3 nm particles in the polluted urban atmosphere of a megacity in China, Atmos. Chem. Phys., 16(4), 2641–2657, doi:10.5194/acp-16-2641-2016, 2016.

Tables

Table 1

Initial concentrations of precursors, reaction rate coefficients, ArHC reacted fraction (%), total HOMs concentration and HOMs yield (%) relative to the reacted ArHC. The mixing ratio of precursors was determined at the exit of the flow tube when the excimer lamp (OH generation) was switched off.

Compound	Concentration (molecules cm^{-3})	k_{OH} (10^{-12} cm^3 $molecules^{-1}$ s^{-1})	Reacted fraction (%)	[HOM] (molecules cm^{-3})	HOMs yield (%)
Benzene (C_6H_6)	$9.85\ 10^{13}$	1.22	0.5	$1.2\ 10^{9}$	0.2
Toluene (C_7H_8)	$1.97\ 10^{13}$	5.63	2.3	$4.4\ 10^{8}$	0.1
Ethylbenzene (C_8H_{10})	$1.13\ 10^{13}$	7.0	4.4	$9.4\ 10^{8}$	0.2
(o/m/p)-xylene (C_8H_{10})	$2.95\ 10^{12}$	13.6/23.1/14.3	5.4 - 9.2	$2.8\ 10^{9}$	1.0 - 1.7
Mesitylene (C_9H_{12})	$2.46\ 10^{12}$	56.7	22.7	$3.1\ 10^{9}$	0.6
Naphthalene ($C_{10}H_8$)	$2.95\ 10^{13}$	23.0	2.6	$1.4\ 10^{10}$	1.8
Biphenyl ($C_{12}H_{10}$)	$4.43\ 10^{13}$	7.1	1.6	$1.8\ 10^{10}$	2.5

Reference for the *k*-rates: Atkinson and Arey, 2003.

Table 2

Summary of HOM characteristics. For each of the 7 compounds the percentage fractional distribution of the signal is presented. For monocyclic compounds the distribution comprises monomers and dimers, for naphthalene and biphenyl monomers, dimers, trimers and tetramers are reported. These values are not quantitative as the instrument cannot be
480 calibrated for such compounds. For each band the weighted arithmetic means of the O:C ratio are reported in parentheses. The fraction of the identified peaks as adduct with NO_3^- is given in the last column.

Compound	Bands distribution				Adduct ($HOM•NO_3^-$)
	Monomer (O:C)		Dimer (O:C)		
Benzene (C_6H_6)	80 (1.08)		20 (0.91)		0.91
Toluene (C_7H_8)	71 (1.09)		29 (0.75)		0.94
Ethylbenzene (C_8H_{10})	69 (0.86)		31 (0.62)		0.83
(o/m/p)-xylene (C_8H_{10})	65 (0.78)		35 (0.57)		0.92
Mesitylene (C_9H_{12})	61 (0.81)		39 (0.49)		0.92
	Monomer (O:C)	Dimer (O:C)	Trimer (O:C)	Tetramer (O:C)	
Naphthalene ($C_{10}H_8$)	34 (0.55)	64 (0.29)	2 (0.34)	1 (0.28)	0.84
Biphenyl ($C_{12}H_{10}$)	52 (0.44)	43 (0.35)	4 (0.29)	1 (0.32)	0.77

485 **Figures**

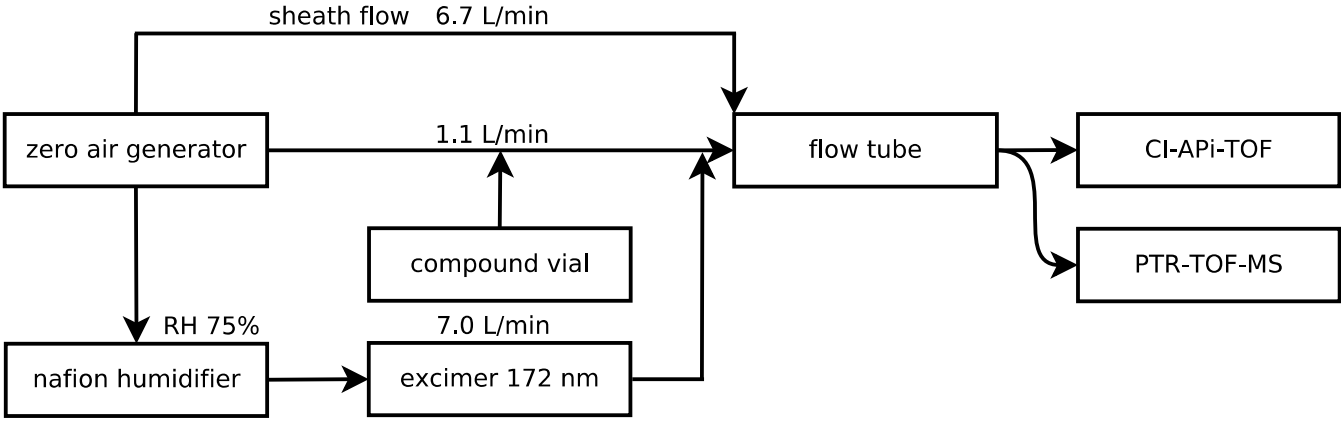

Figure 1. Experimental set-up. Zero air from a pure air generator is split into 3 flows. A sheath flow of 6.7 L min^{-1}. An air stream of 1.1 L min^{-1} collects vapors from a reagent compound vial and is then mixed with a humidified air stream of 7 L min^{-1} (RH 75%) which carries OH free radicals generated through irradiation at 172 nm.

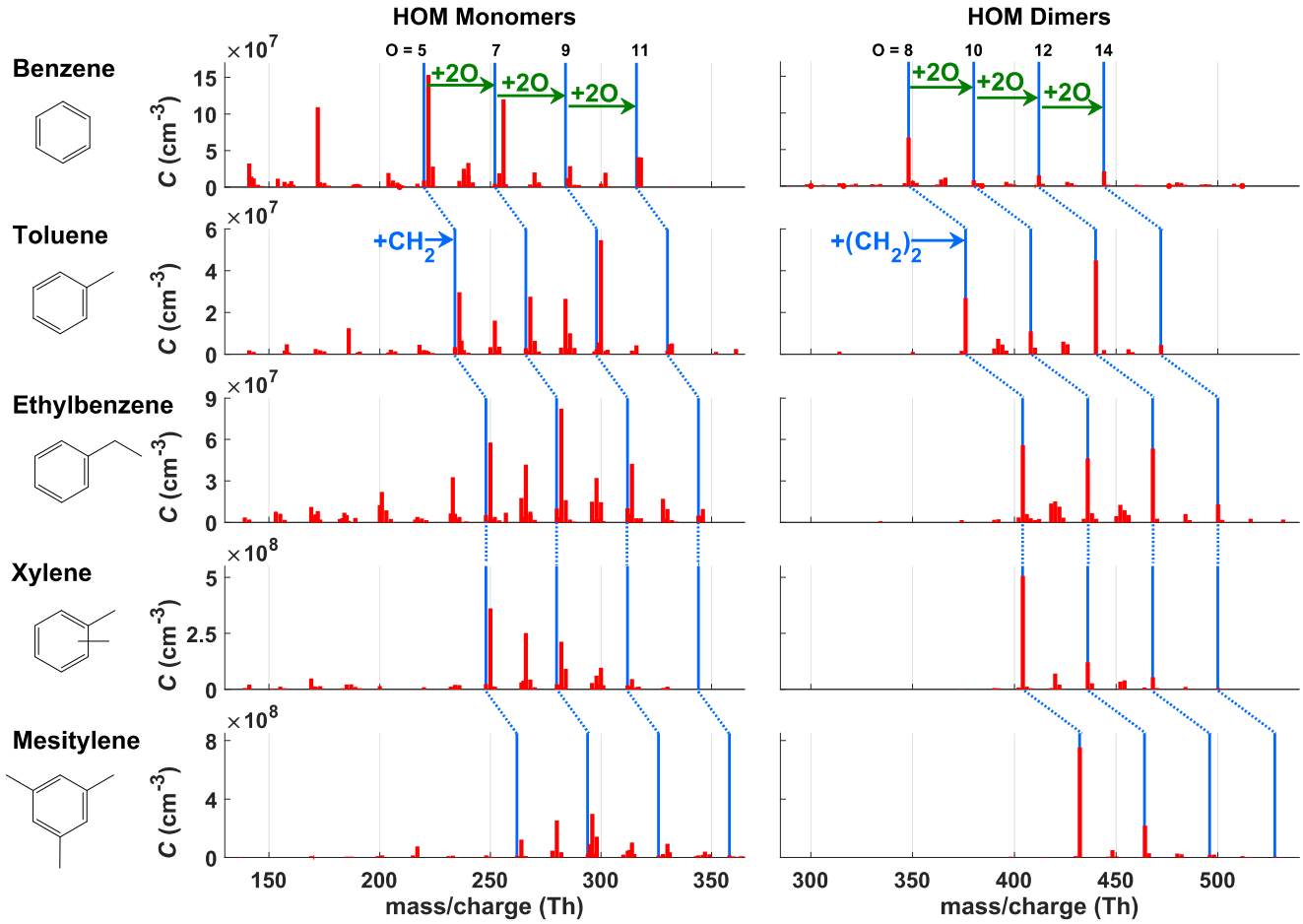

Figure 2. HOMs from 5 monocyclic ArHC (benzene, toluene, ethylbenzene, xylenes, mesitylene). HOM monomers (left panel) have the same number of carbon atoms as the precursor while HOM dimers (right panel) have twice as many. Green arrows in the benzene panel show a sequence of peaks separated by a mass corresponding to 2 oxygen atoms. This may be connected to the autoxidation mechanism which proceeds through addition of O_2 molecules. The same sequence is seen in the other ArHCs as indicated by the blue lines. The initial peak and the corresponding sequence of the 5 single-ring ArHC are shifted by a CH_2 unit due to the different substituents (blue arrow in the toluene panel). HOMs with the same number of oxygen atoms can have a different number of hydrogen atoms (n, n+2, n+4). Note the different peak intensity patterns observed for the different chemical compounds, even for xylene and ethylbenzene, i.e., molecules with the same chemical formula.

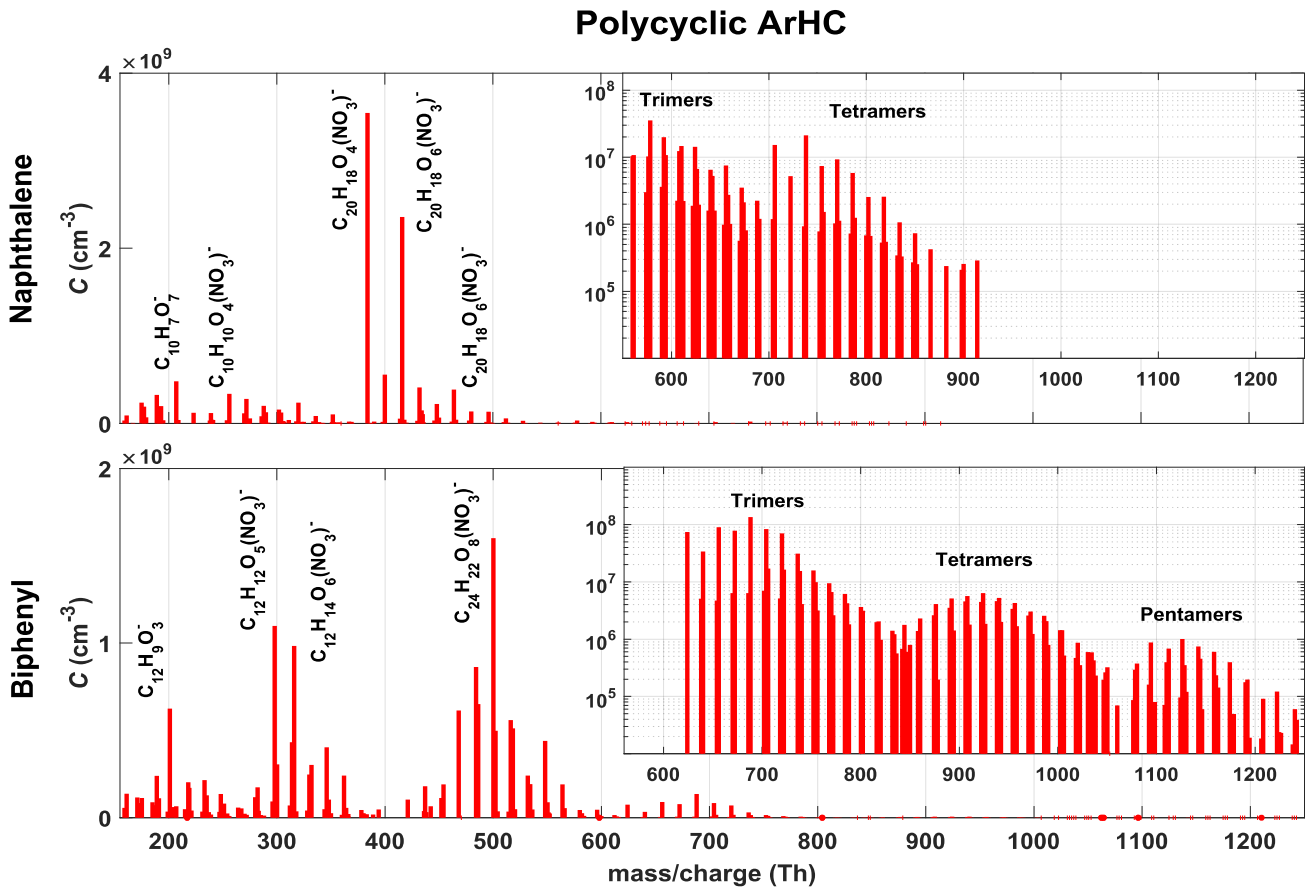

Figure 3. Mass spectra of HOMs from the bicyclic ArHC naphthalene and biphenyl. The chemical composition of some representative peaks is displayed. Due to the high concentrations the nitrate CI-APi-TOF was also able to detect the HOMs clusters up to the pentamer and also retrieve their chemical formula (see inserts).

505

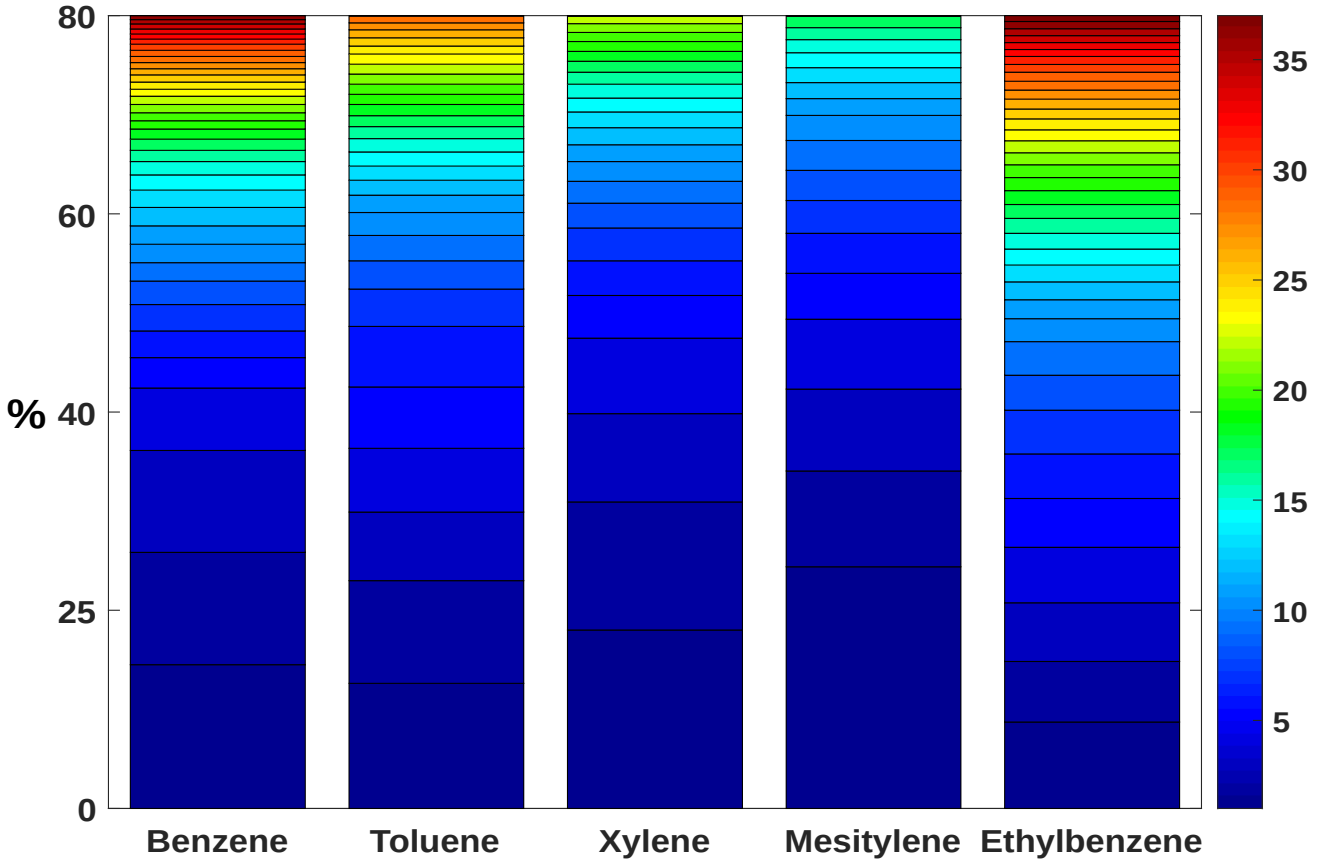

Figure 4. Graphical representation of the cumulative peak lists for the 5 monocyclic ArHC. The bar plot shows the cumulative contribution of the most abundant HOMs species to 80% of the total detected signal for each single-ring ArHC. Each colour of the stacked bar plots denotes a certain number of cumulative compounds. In the series benzene, toluene, xylene and mesitylene a gradually smaller number of different HOM species is needed to explain 80% of the total signal. However, this trend with the increase of the number of substituents is not met by ethylbenzene. This may be linked to the fact that dimers with an unexpectedly low number of hydrogen were observed. Ethylbenzene shows a lower fraction of HOM·NO_3^- adducts as well.

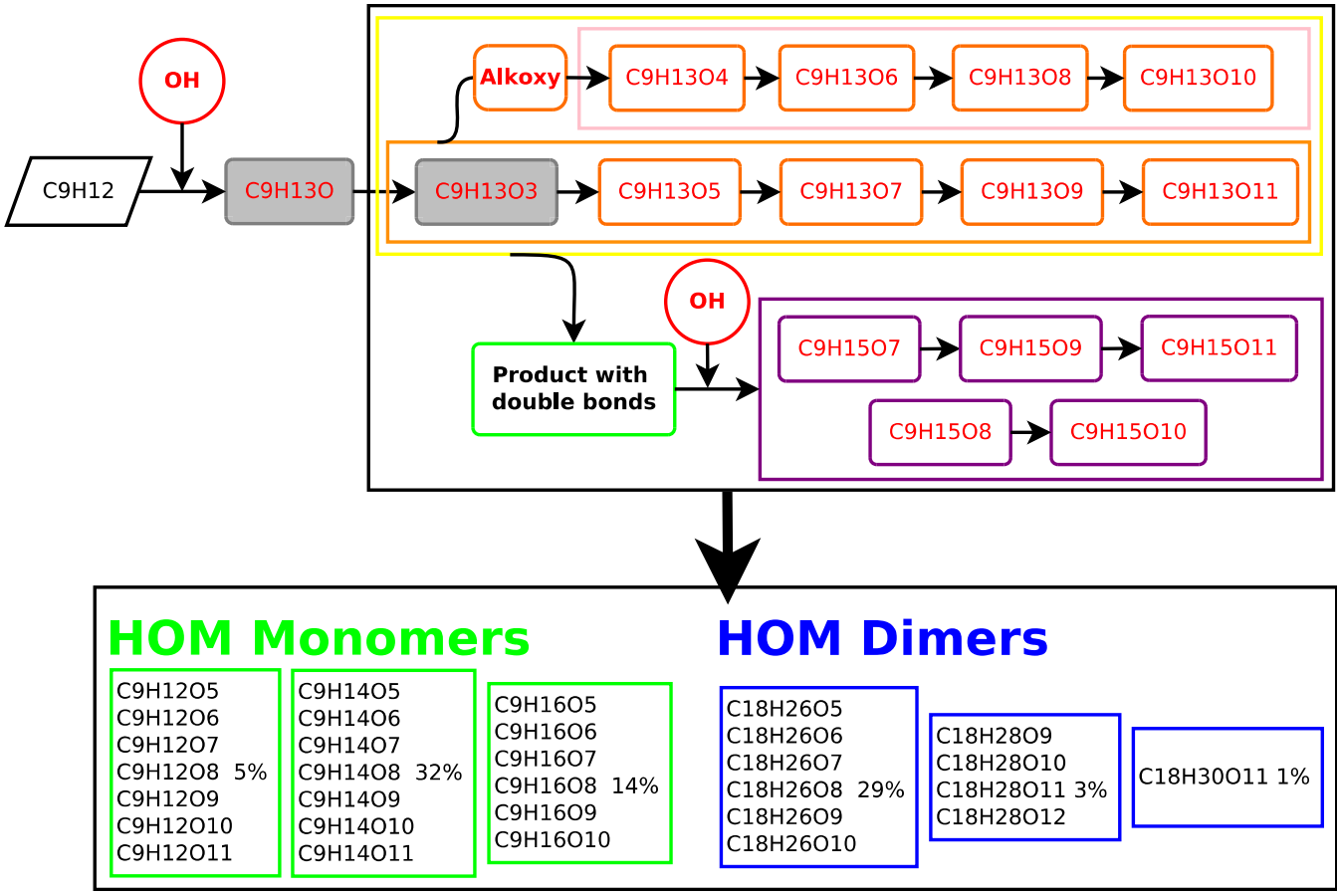

Figure 5 Proposed generalized reaction scheme of HOM formation for mesitylene (1,3,5-trimethylbenzene) after OH addition. In black closed-shell species (even number of H), in red radicals (odd number of H). Grey colour denotes radicals that were not detected by the CIMS. Radicals in the orange box are from the propagation of the initial OH attack with an odd number of oxygen atoms, radicals in the pink box are formed via an alkoxy intermediate step with an even number of oxygen atoms, while radicals in the purple box are products of a second OH addition. Reacting oxygen molecules along the radical propagation chain are not indicated. Closed-shell species are divided into monomers (green boxes) and dimers (blue boxes). The percentages in the boxes indicate the relative intensity of a peak to the total detected ArHC HOMs signal. The sum does not add up to 100% because some peaks mainly coming from fragmentation are not included in the scheme.

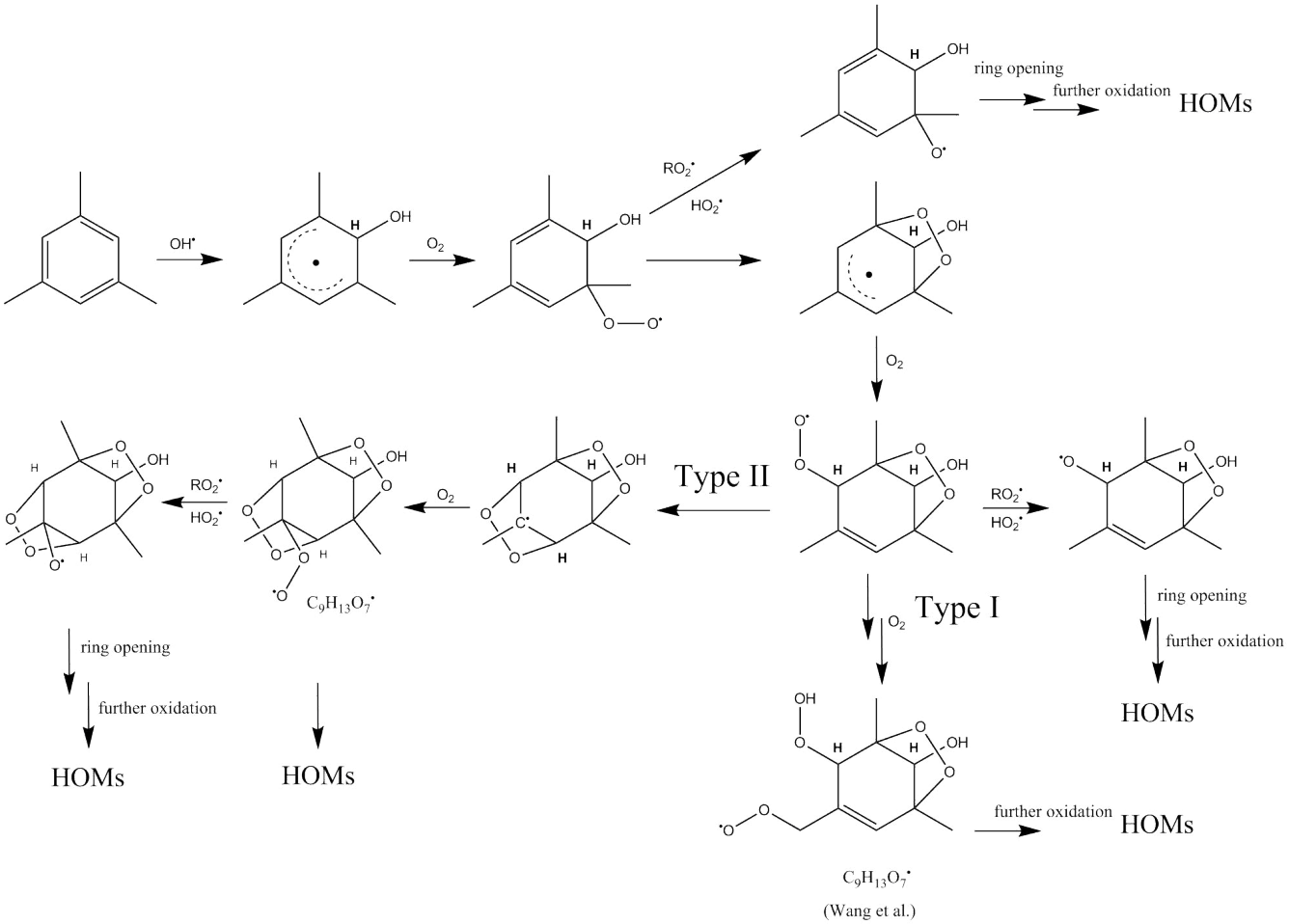

Figure 6. Proposed radical reaction mechanism for the autoxidation of mesitylene. The mechanism is derived from the MCM (version 3.3.1) up to the $C_9H_{13}O_5$ radical. From there the Type I pathway is from Wang et al., (2017).

530

Appendix A

Peak lists of the most abundant HOMs of each ArHC tested are presented in the next 7 tables. The peaks are sorted according to decreasing relative intensity. Chemical formula, exact mass and fraction of the explained signal are included. The exact mass includes the mass of NO_3 if present.

Table A-1

CI-APi-TOF peak list for benzene (C_6H_6) oxidation products.

Chemical formula	Mass	Fraction of explained signal
$C_6H_8O_5(NO_3)^-$	222.0255	14.1
$C_5H_6O_8(NO_3)^-$	255.9946	11.0
$C_6H_6O_2(NO_3)^-$	172.0251	10.0
$C_{12}H_{14}O_8(NO_3)^-$	348.0572	6.1
$C_5H_6O_7(NO_3)^-$	239.9997	3.0
$C_6H_8O_9(NO_3)^-$	286.0052	2.6
$C_5H_6O_6(NO_3)^-$	224.0048	2.6
$C_6H_8O_6(NO_3)^-$	238.0205	2.3
$C_6H_8O_8(NO_3)^-$	270.0103	1.8
$C_{12}H_{14}O_{14}(NO_3)^-$	444.0267	1.8
$C_6H_8O_{10}(NO_3)^-$	302.0001	1.8
$C_6H_6O_4(NO_3)^-$	204.0150	1.8
$C_6H_8O_7(NO_3)^-$	254.0154	1.7
$C_6H_{10}O_6(NO_3)^-$	240.0361	1.5
$C_{12}H_{14}O_{12}(NO_3)^-$	412.0369	1.3
$C_6H_7O_9(NO_3)^-$	284.9974	1.1
$C_6H_7O_4^-$	143.0350	1.1
$C_{12}H_{16}O_9(NO_3)^-$	366.0678	1.0
$C_6H_8O_4(NO_3)^-$	206.0306	0.8
$C_6H_6O_5(NO_3)^-$	220.0099	0.8
$C_{12}H_{14}O_9(NO_3)^-$	364.0522	0.8
$C_6H_6O_6(NO_3)^-$	236.0048	0.8
$C_5H_6O_2(NO_3)^-$	160.0251	0.7
$C_{12}H_{14}O_{10}(NO_3)^-$	380.0471	0.7
$C_6H_5O_5^-$	157.0143	0.7
$C_{12}H_{16}O_8(NO_3)^-$	350.0729	0.6
$C_6H_5O_6^-$	173.0092	0.6
$C_5H_8O_7(NO_3)^-$	242.0154	0.6
$C_6H_{10}O_8(NO_3)^-$	272.0259	0.6
$C_5H_6O_5(NO_3)^-$	208.0099	0.6
$C_{12}H_{14}O_{11}(NO_3)^-$	396.0420	0.5
$C_{12}H_{12}O_{13}(NO3)^-$	426.0161	0.5
$C_6H_7O_6^-$	175.0248	0.5
$C_{10}H_{10}O_{18}(NO_3)^-$	479.9751	0.5

$C_6H_7O_4(NO_3)^-$	205.0228	0.4
$C_6H_6O_7(NO_3)^-$	251.9997	0.4

540

Table A-2

CI-APi-TOF peak list for toluene (C_7H_8) oxidation products.

Chemical formula	Mass	Fraction of explained signal
$C_7H_{10}O_9(NO_3)^-$	300.0208	12.4
$C_{14}H_{18}O_{12}(NO_3)^-$	440.0682	10.2
$C_7H_{10}O_5(NO_3)^-$	236.0412	6.8
$C_7H_{10}O_7(NO_3)^-$	268.0310	6.3
$C_{14}H_{18}O_8(NO_3)^-$	376.0885	6.1
$C_7H_{10}O_8(NO_3)^-$	284.0259	6.0
$C_7H_{10}O_6(NO_3)^-$	252.0361	3.7
$C_7H_8O_2(NO_3)^-$	186.0408	2.8
$C_{14}H_{18}O_{10}(NO_3)^-$	408.0784	2.5
$C_7H_{12}O_8(NO_3)^-$	286.0416	2.3
$C_{14}H_{18}O_9(NO_3)^-$	392.0834	1.7
$C_6H_7O_6(NO_3)^-$	237.0126	1.5
$C_7H_{12}O_7(NO_3)^-$	270.0467	1.4
$C_{14}H_{18}O_{11}(NO_3)^-$	424.0733	1.4
$C_7H_9O_9(NO_3)^-$	299.0130	1.3
$C_7H_{10}O_{11}(NO_3)^-$	332.0107	1.2
$C_7H_9O_{11}(NO_3)^-$	331.0029	1.1
$C_6H_6O_5^-$	158.0215	1.1
$C_{14}H_{20}O_{11}(NO_3)^-$	426.0889	1.1
$C_{14}H_{20}O_9(NO_3)^-$	394.0991	1.0
$C_7H_8O_4(NO_3)^-$	218.0306	1.0
$C_6H_8O_8(NO_3)^-$	270.0103	1.0
$C_{14}H_{18}O_{14}(NO_3)^-$	472.0580	1.0
$C_7H_{10}O_{10}(NO_3)^-$	316.0158	1.0
$C_7H_{12}O_6(NO_3)^-$	254.0518	0.8
$C_7H_8O_5(NO_3)^-$	234.0255	0.8
$C_7H_8O_6(NO_3)^-$	250.0205	0.8
$C_{14}H_{20}O_{10}(NO_3)^-$	410.0940	0.7
$C_7H_8O_8(NO_3)^-$	282.0103	0.7

Table A-3

CI-APi-TOF peak list for ethylbenzene (C_8H_{10}) oxidation products.

Chemical formula	Mass	Fraction of explained signal
$C_8H_{12}O_7(NO_3)^-$	282.0467	8.7
$C_8H_{12}O_5(NO_3)^-$	250.0568	6.1
$C_{16}H_{22}O_8(NO_3)^-$	404.1198	5.9
$C_{16}H_{22}O_{12}(NO_3)^-$	468.0995	5.6
$C_{16}H_{22}O_{10}(NO_3)^-$	436.1096	4.9
$C_8H_{12}O_9(NO_3)^-$	314.0365	4.5
$C_8H_{12}O_6(NO_3)^-$	266.0518	4.4
$C_8H_9O_8^-$	233.0303	3.5
$C_8H_{12}O_8(NO_3)^-$	298.0416	3.4
$C_8H_9O_6^-$	201.0405	2.3
$C_8H_{10}O_6(NO_3)^-$	264.0361	1.9
$C_8H_{10}O_{10}(NO_3)^-$	328.0158	1.8
$C_8H_{14}O_7(NO_3)^-$	284.0623	1.7
$C_{16}H_{22}O_9(NO_3)^-$	420.1147	1.6
$C_8H_{10}O_8(NO_3)^-$	296.0259	1.6
$C_8H_{14}O_8(NO_3)^-$	300.0572	1.5
$C_{16}H_{20}O_9(NO_3)^-$	418.0991	1.4
$C_{16}H_{22}O_{14}(NO_3)^-$	500.0893	1.4
$C_{16}H_{22}O_{11}(NO_3)^-$	452.1046	1.3
$C_8H_{10}O_2(NO_3)^-$	200.0564	1.3
$C_{16}H_{24}O_9(NO_3)^-$	422.1304	1.2
$C_8H_9O_4^-$	169.0506	1.2
$C_8H_{10}O_9(NO_3)^-$	312.0208	1.1
$C_8H_{10}O_7(NO_3)^-$	280.0310	1.1
$C_8H_{12}O_{11}(NO_3)^-$	346.0263	1.0
$C_8H_{12}O_{10}(NO_3)^-$	330.0314	1.0
$C_8H_{11}O_6^-$	203.0561	0.9
$C_{16}H_{24}O_{11}(NO_3)^-$	454.1202	0.9
$C_7H_8O_5^-$	172.0377	0.9
$C_8H_9O_3^-$	153.0557	0.8
$C_8H_{14}O_6(NO_3)^-$	268.0674	0.8
$C_8H_8O_5^-$	184.0377	0.7
$C_{16}H_{24}O_{10}(NO_3)^-$	438.1253	0.7
$C_8H_{10}O_4(NO_3)^-$	232.0463	0.7
$C_7H_8O_5(NO_3)^-$	234.0255	0.7
$C_8H_{11}O_9(NO_3)^-$	313.0287	0.7
$C_7H_7O_4^-$	155.0350	0.6

Table A-4

CI-APi-TOF peak list for xylene (C_8H_{10}) oxidation products.

Chemical formula	Mass	Fraction of explained signal
$C_{16}H_{22}O_8(NO_3)^-$	404.1198	18.0
$C_8H_{12}O_5(NO_3)^-$	250.0568	12.9
$C_8H_{12}O_6(NO_3)^-$	266.0518	8.9
$C_8H_{12}O_7(NO_3)^-$	282.0467	7.6
$C_{16}H_{22}O_{10}(NO_3)^-$	436.1096	4.3
$C_8H_{14}O_8(NO_3)^-$	300.0572	3.5
$C_8H_{14}O_7(NO_3)^-$	284.0623	3.3
$C_{16}H_{22}O_9(NO_3)^-$	420.1147	2.5
$C_8H_{12}O_8(NO_3)^-$	298.0416	2.2
$C_{16}H_{22}O_{12}(NO_3)^-$	468.0995	2.0
$C_8H_9O_4^-$	169.0506	1.7
$C_8H_{12}O_9(NO_3)^-$	314.0365	1.7
$C_8H_{14}O_6(NO_3)^-$	268.0674	1.6
$C_{16}H_{24}O_{11}(NO_3)^-$	454.1202	1.4
$C_8H_{11}O_6(NO_3)^-$	265.0439	1.4
$C_{16}H_{22}O_{11}(NO_3)^-$	452.1046	1.2
$C_8H_{10}O_6(NO_3)^-$	264.0361	1.1
$C_8H_{10}O_8(NO_3)^-$	296.0259	1.0
$C_{16}H_{24}O_{10}(NO_3)^-$	438.1253	1.0
$C_8H_{10}O_5(NO_3)^-$	248.0412	0.9
$C_8H_{13}O_8(NO_3)^-$	299.0494	0.9
$C_8H_{10}O_7(NO_3)^-$	280.0310	0.8

Table A-5

CI-APi-TOF peak list for mesitylene (C_9H_{12}) oxidation products.

Chemical formula	Mass	Fraction of explained signal
$C_{18}H_{26}O_8(NO_3)^-$	432.1511	24.2
$C_9H_{14}O_7(NO_3)^-$	296.0623	9.6
$C_9H_{14}O_6(NO_3)^-$	280.0674	8.2
$C_{18}H_{26}O_{10}(NO_3)^-$	464.1410	7.0
$C_9H_{16}O_7(NO_3)^-$	298.0780	4.6
$C_9H_{14}O_5(NO_3)^-$	264.0725	4.0
$C_9H_{16}O_8(NO_3)^-$	314.0729	3.3
$C_9H_{16}O_9(NO_3)^-$	330.0679	3.0
$C_9H_{13}O_7(NO_3)^-$	295.0545	3.0
$C_9H_{13}O_6^-$	217.0718	2.5
$C_9H_{15}O_8(NO_3)^-$	313.0651	1.7
$C_{18}H_{26}O_9(NO_3)^-$	448.1461	1.6
$C_9H_{14}O_8(NO_3)^-$	312.0572	1.5
$C_9H_{12}O_6(NO_3)^-$	278.0518	1.5
$C_9H_{17}O_{10}(NO_3)^-$	347.0705	1.3
$C_9H_{14}O_{10}^-$	282.0592	1.2
$C_9H_{17}O_9(NO_3)^-$	331.0756	1.2

555

Table A-6

CI-APi-TOF peak list for naphthalene ($C_{10}H_8$) oxidation products.

Chemical formula	Mass	Fraction of explained signal
$C_{20}H_{18}O_4(NO_3)^-$	384.1089	26.1
$C_{20}H_{18}O_6(NO_3)^-$	416.0987	17.4
$C_{20}H_{18}O_5(NO_3)^-$	400.1038	4.1
$C_{10}H_7O_5^-$	207.0299	3.5
$C_{20}H_{18}O_7(NO_3)^-$	432.0936	3.0
$C_{20}H_{18}O_9(NO_3)^-$	464.0834	2.9
$C_{10}H_{10}O_4(NO_3)^-$	256.0463	2.5
$C_{10}H_{10}O_5(NO_3)^-$	272.0412	2.1
$C_{10}H_7O_3^-$	175.0401	1.8
$C_{10}H_{10}O_8(NO_3)^-$	320.0259	1.7
$C_{20}H_{18}O_8(NO_3)^-$	448.0885	1.6
$C_{10}H_{10}O_6(NO_3)^-$	288.0361	1.5
$C_{10}H_8O_7(NO_3)^-$	302.0154	1.2
$C_{20}H_{20}O_7(NO_3)^-$	434.1093	1.1
$C_{10}H_7O_4^-$	191.0350	1.0
$C_{20}H_{18}O_{10}(NO_3)^-$	480.0784	1.0
$C_{20}H_{18}O_{11}(NO_3)^-$	496.0733	1.0
$C_{10}H_{12}O_6(NO_3)^-$	290.0518	0.9
$C_{10}H_{10}O_7(NO_3)^-$	304.0310	0.9
$C_{10}H_7O_6^-$	223.0248	0.9
$C_{10}H_7O_7^-$	239.0197	0.9
$C_{10}H_8O_5(NO_3)^-$	270.0255	0.9
$C_{10}H_{10}O_{10}(NO_3)^-$	352.0158	0.8
$C_{10}H_{10}O_9(NO_3)^-$	336.0208	0.6

560

Table A-7

CI-APi-TOF peak list for biphenyl ($C_{12}H_{10}$) oxidation products.

Chemical formula	Mass	Fraction of explained signal
$C_{24}H_{22}O_8(NO_3)^-$	500.1198	9.1
$C_{12}H_{12}O_5(NO_3)^-$	298.0569	6.2
$C_{12}H_{14}O_6(NO_3)^-$	316.0674	5.6
$C_{24}H_{22}O_7(NO_3)^-$	484.1249	4.9
$C_{24}H_{24}O_7(NO_3)^-$	486.1406	3.7
$C_{12}H_9O_4^-$	217.0506	3.6
$C_{12}H_9O_3^-$	201.0557	3.5
$C_{24}H_{22}O_6(NO_3)^-$	468.1300	3.5
$C_{24}H_{22}O_9(NO_3)^-$	516.1147	3.2
$C_{24}H_{24}O_9(NO_3)^-$	518.1304	2.9
$C_{24}H_{24}O_8(NO_3)^-$	502.1355	2.8
$C_{24}H_{22}O_{11}(NO_3)^-$	548.1046	2.5
$C_{12}H_{12}O_6(NO_3)^-$	314.0518	2.4
$C_{12}H_{12}O_8(NO_3)^-$	346.0416	2.3
$C_{12}H_{14}O_5(NO_3)^-$	300.0725	1.7
$C_{12}H_{14}O_7(NO_3)^-$	332.0623	1.7
$C_{12}H_{12}O_7(NO_3)^-$	330.0467	1.4
$C_{24}H_{22}O_{10}(NO_3)^-$	532.1097	1.4
$C_{12}H_{12}O_9(NO_3)^-$	362.0365	1.4
$C_{11}H_9O_3^-$	189.0557	1.4
$C_{12}H_9O_5^-$	233.0455	1.2
$C_{12}H_{10}O_4^-$	218.0585	1.1
$C_{24}H_{24}O_{10}(NO_3)^-$	534.1253	1.1
$C_{24}H_{24}O_5(NO_3)^-$	454.1507	1.1
$C_{24}H_{22}O_{12}(NO_3)^-$	564.0995	1.1
$C_{24}H_{21}O_8^-$	437.1242	1.0
$C_{12}H_{12}O_4(NO_3)^-$	282.0619	1.0
$C_{12}H_{11}O_4^-$	219.0663	1.0
$C_{10}H_9O_2^-$	161.0608	0.8
$C_{12}H_{10}O_2(NO_3)^-$	248.0564	0.8
$C_{36}H_{34}O_{10}(NO_3)^-$	688.2036	0.8
$C_{12}H_{11}O_5^-$	235.0612	0.7
$C_{12}H_{10}O_4(NO_3)^-$	280.0463	0.7
$C_{11}H_7O_2^-$	171.0452	0.7
$C_{24}H_{22}O_5(NO_3)^-$	452.1351	0.6
$C_{10}H_7O_3^-$	175.0401	0.6
$C_{10}H_7O_4^-$	191.0350	0.6

Appendix B

HOMs from the 7 tested compounds are presented in the next figures. Top panel left: pie chart showing the monomer and dimer fraction; 3 bar plots presenting the relative signal intensities for radicals, monomer and dimers. In the bar plots, the x axis presents the number of oxygen atoms and the colour code the number of hydrogen atoms for each of the HOMs.

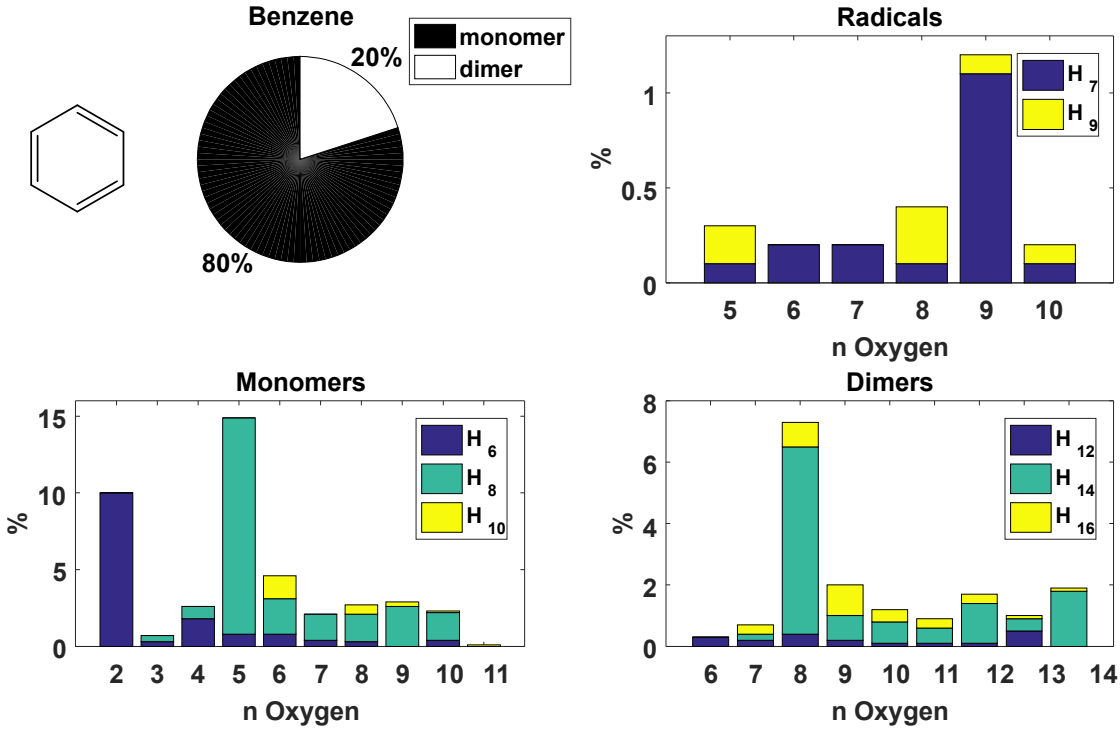

Figure B – 1 Benzene

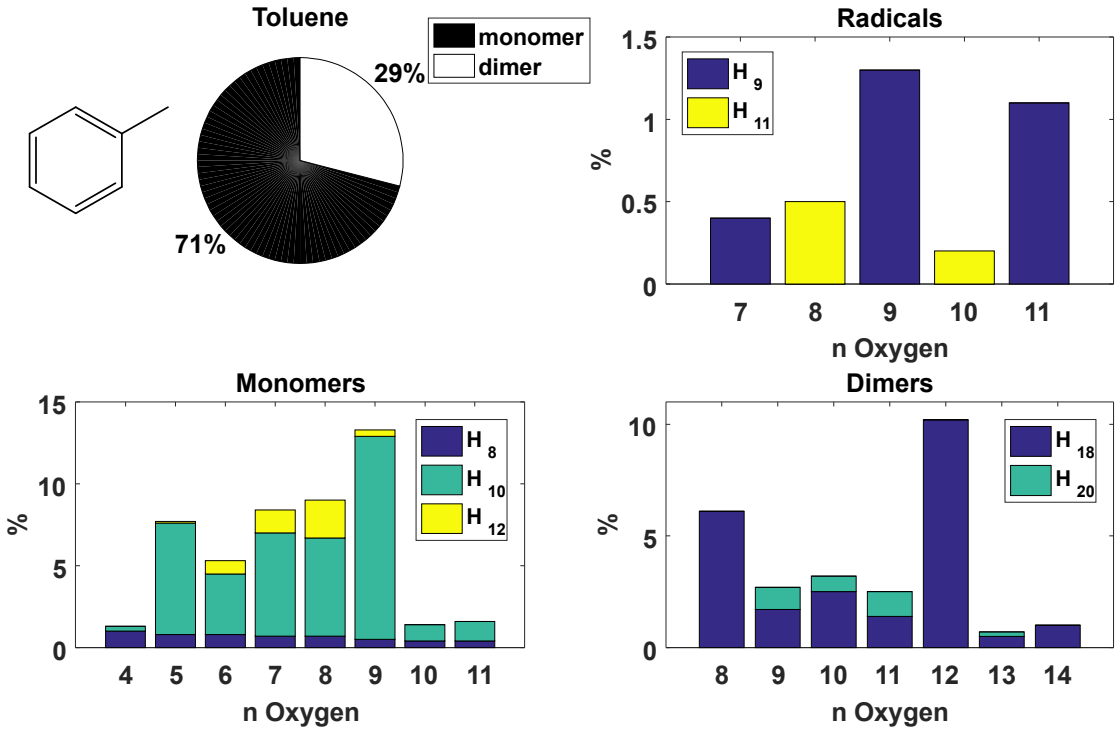

Figure B – 2 Toluene

575

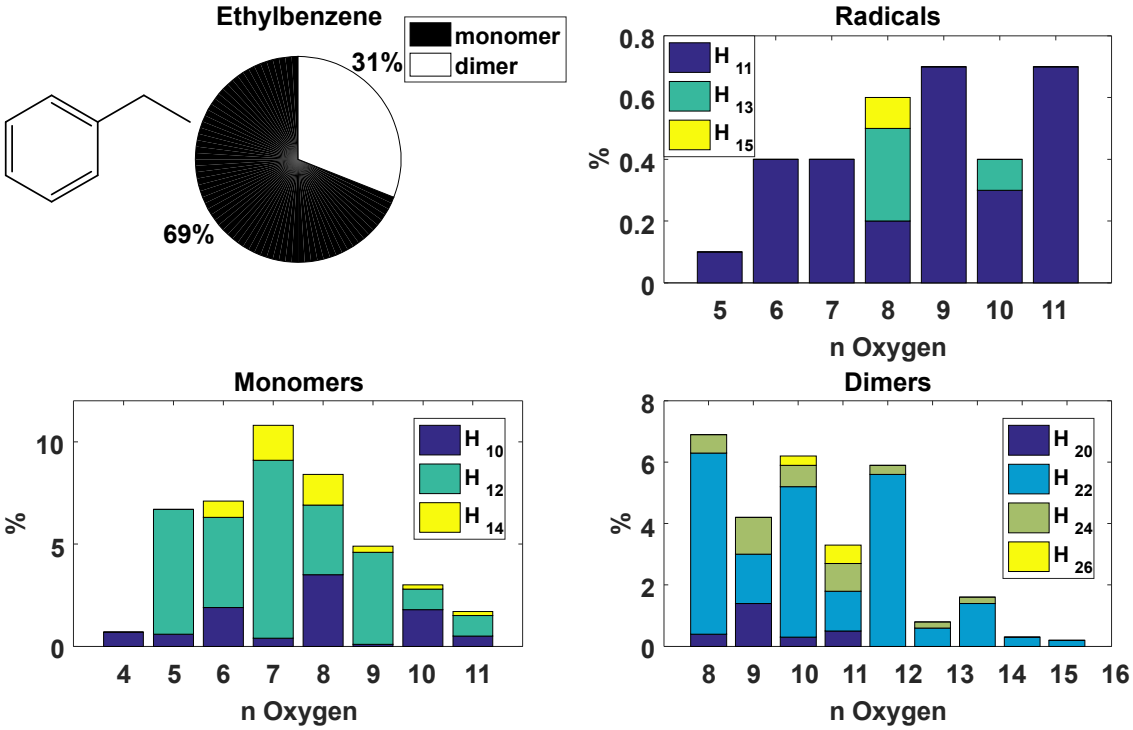

Figure B – 3 Ethylbenzene

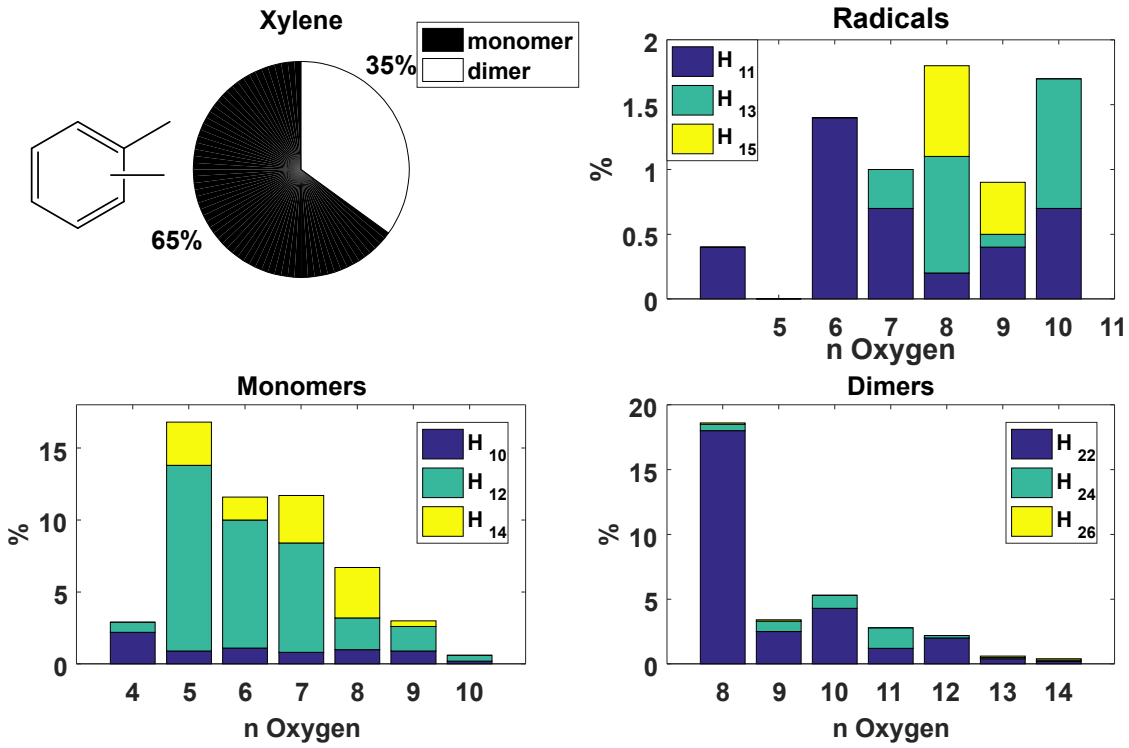

580 Figure B – 4 Xylene

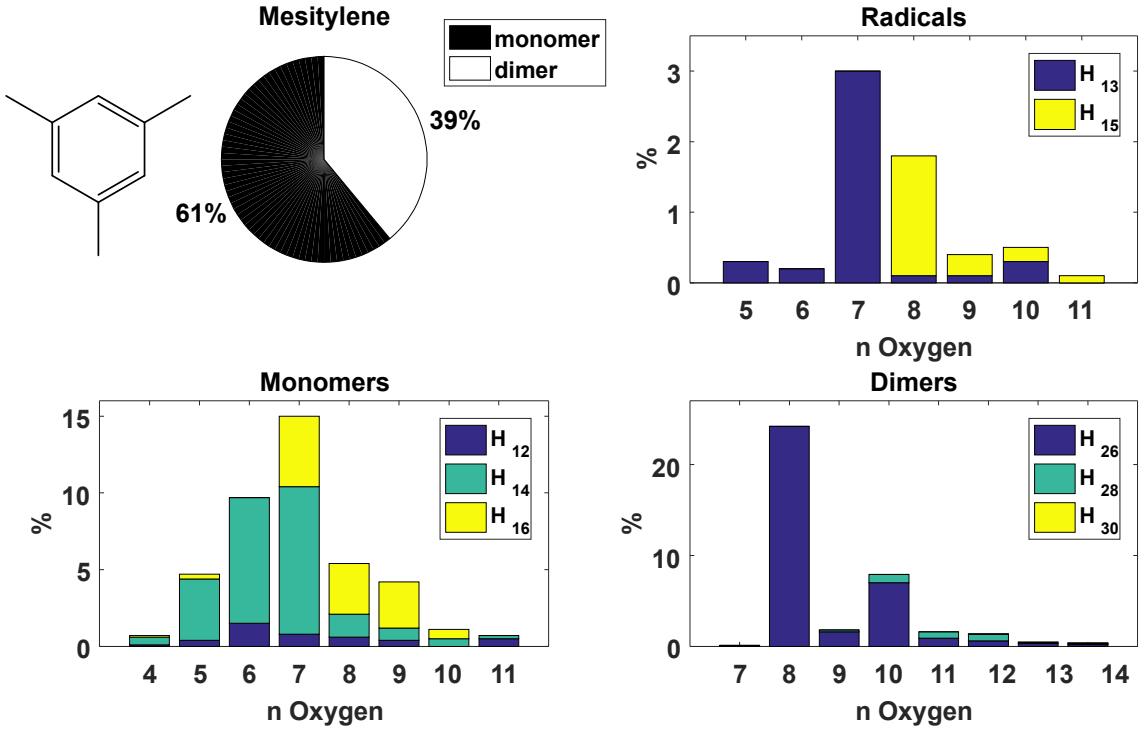

Figure B – 5 Mesitylene

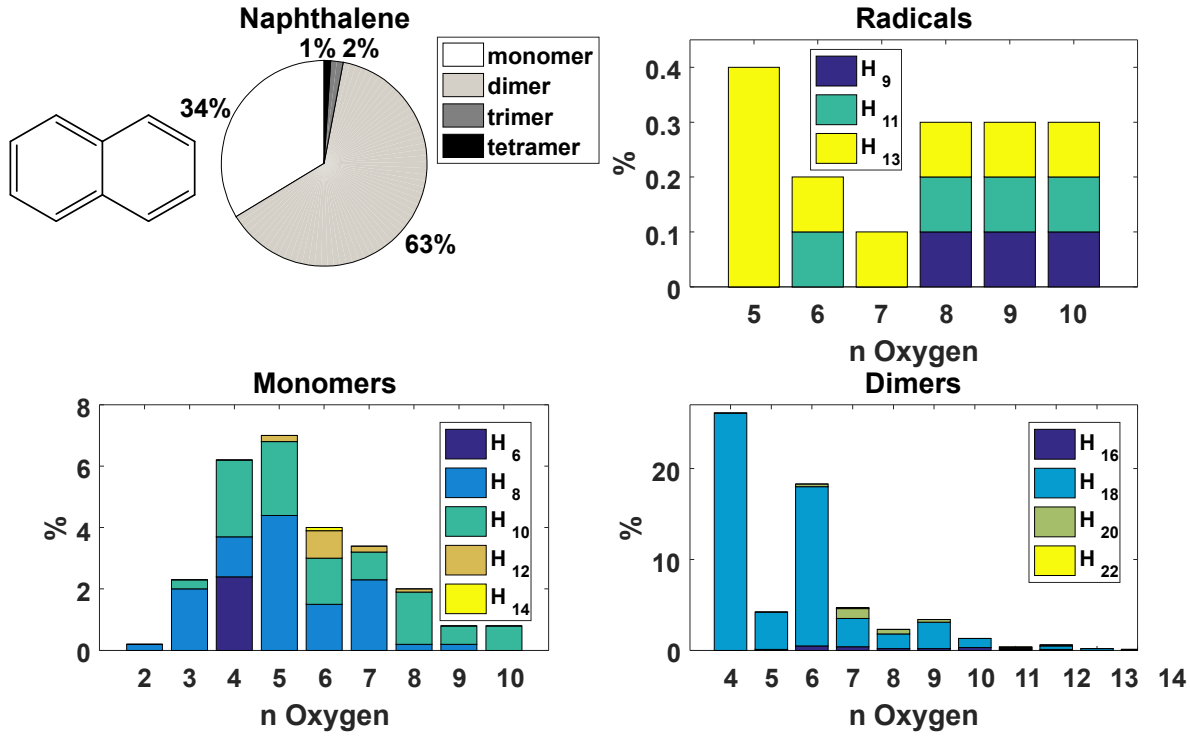

585 Figure B – 6 Naphthalene

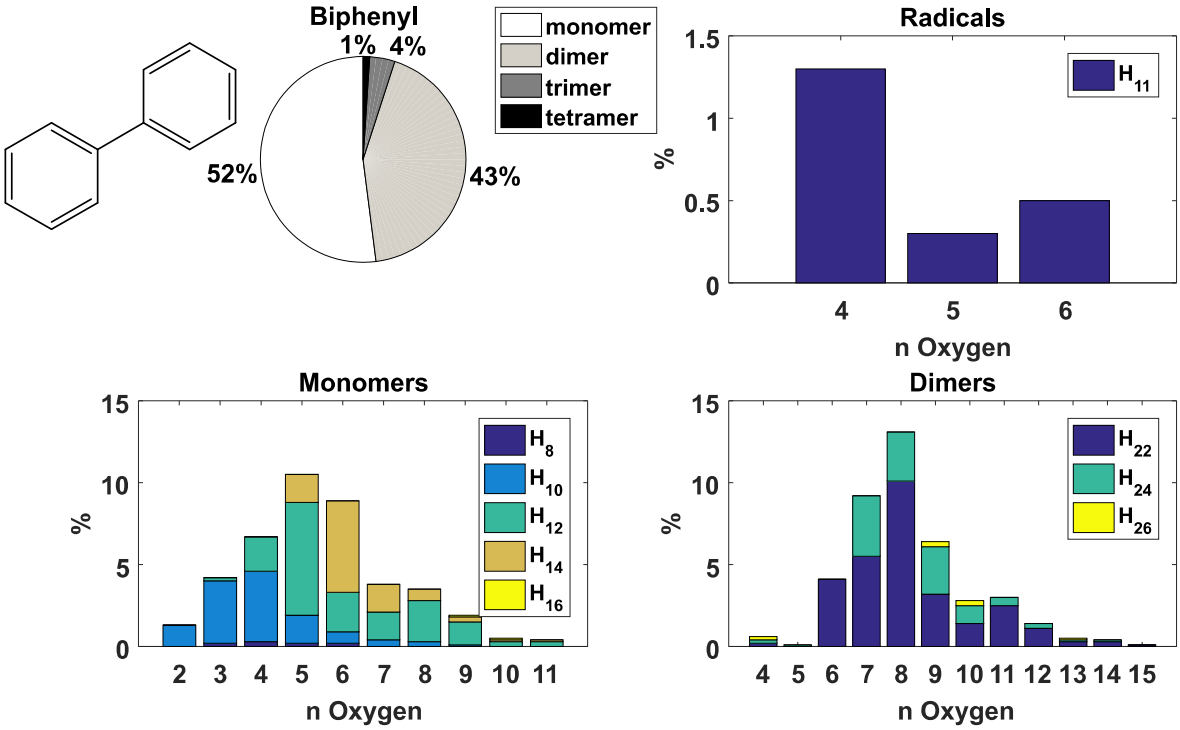

Figure B – 7 Biphenyl

Appendix C

Here a description of the OH generator and the involved reactions is given. A kinetic reaction model was developed to investigate the effect of uncertainties in the initial OH concentration on the oxidation product distribution.

The radiation at 172 nm excites molecular oxygen and water vapor triggering the following radical reactions:

$h\nu + O_2$	→	$O(^1D) + O(^3P)$	(R-C1)
$O(^1D) + M$	→	$O(^3P) + M$	(R-C2)
$O(^3P) + O_2 + M$	→	$O_3 + M$	(R-C3)
$O(^1D) + H_2O$	→	2 OH	(R-C4)
$h\nu + H_2O$	→	H + OH	(R-C5)
$H + O_2 + M$	→	$HO_2 + M$	(R-C6)
$OH + O_3$	→	$HO_2 + O_2$	(R-C7)
$HO_2 + O_3$	→	$OH + 2O_2$	(R-C8)
$OH + HO_2$	→	$H_2O + O_2$	(R-C9)
$HO_2 + HO_2$	→	$H_2O_2 + O_2$	(R-C10)
$H_2O_2 + OH$	→	$H_2O + HO_2$	(R-C11)

The humidified air flow is exposed to the 172 nm radiation for 50 ms and is then within 30 ms transferred to the mixing zone with the sample flow. The oxidant species produced are OH, HO_2, O_3 and H_2O_2. The final OH concentration entering the mixing zone depends on the residence time of the air in the lamp and in the transfer region.

The kinetic model includes 31 species and 36 reactions from the MCM 3.3.1 (Jenkin et al., 2003). Mesitylene is selected as ArHC for these simulations and its reaction mechanism is extended up to the second generation products. The model is run for 20 seconds in agreement with the residence time of the flow tube reactor with a simulation time resolution of 2 ms. The model is initiated with the measured concentrations of ozone ($3.45\ 10^{12}$ molecules cm^{-3} without mesitylene) and mesitylene ($2.46\ 10^{12}$ molecules cm^{-3} without lamp on) at the exit of the flow tube. The initial OH radical concentration ($8.50\ 10^{11}$ molecules cm^{-3}) is tuned in order to match the OH exposure, which was determined from the amount of reacted mesitylene. The initial HO_2 radical concentration ($1.70\ 10^{12}$ molecules cm^{-3}) is set at twice the initial OH radical concentration. Wall losses of about 35% are estimated for mesitylene HOMs but are not implemented in the model. Figure C1 shows the temporal evolution of 6 selected species: reacted mesitylene (T135MB reacted), HO_2 radical (HO2), OH radical (OH) as well as 3 products of the mesitylene oxidation with the OH radical (TM135BPRO2, TM135BPOOH and TM135B2OH). TM135BPRO2 is an intermediate peroxy radical after OH attack; TM135BPOOH is a product from the reaction of TM135BPRO2 with the HO_2 radical while TM135BPO2OH is a product from the reaction of TM135BPRO2 with a peroxy radical RO_2. Mesitylene reacted reaches a plateau after about 0.03 seconds while TM135BPRO2 reaches a maximum value around 0.01-0.02 seconds and then rapidly decreases. The closed shell products TM135BPOOH and TM135BPO2OH constantly increase and reach a plateau after about 0.4-1.0 seconds. A similar trend could be expected for HOMs assuming that TM135BPRO2 undergoes an autoxidation chain and is terminated either by HO_2 or by RO_2. In a test run where the

initial mesitylene concentration and the reaction rate constant towards OH radicals were doubled, the ratio TM135BPOOH/TM135BPO2OH varied only by about 18%.

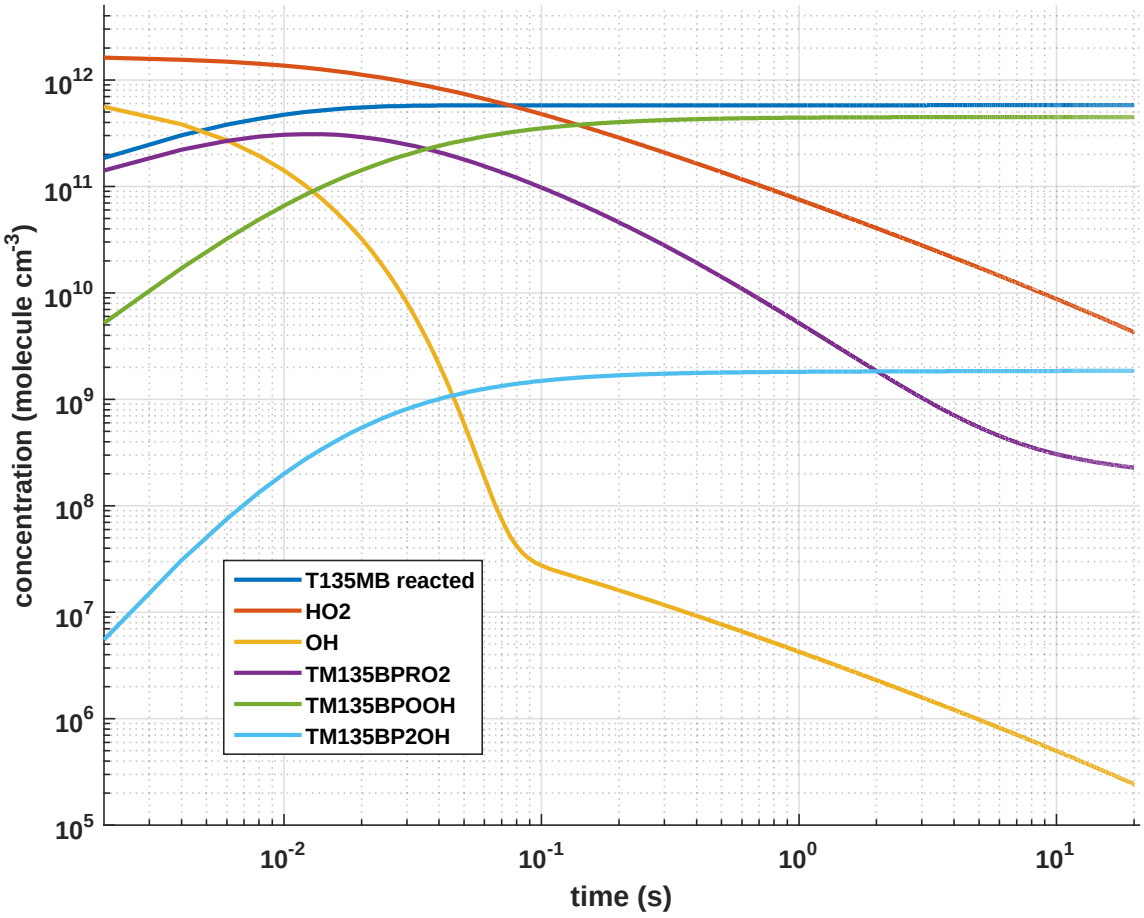

Figure C1. Temporal evolution of selected species according to the mesitylene flow tube kinetic model.